Bulletin of the Seismological Society of America, Vol. 104, No. 1, pp. 301–320, February 2014, doi: 10.1785/0120110277

Ⓔ

Earthquake Ground Motion and 3D Georgia Basin Amplification in Southwest British Columbia: Deep Juan de Fuca Plate Scenario Earthquakes

by Sheri Molnar,* John F. Cassidy,† Kim B. Olsen, Stan E. Dosso, and Jiangheng He

Abstract Finite-difference modeling of 3D long-period (> 2 s) ground motions for large (M_w 6.8) scenario earthquakes is conducted to investigate effects of the Georgia basin structure on ground shaking in Greater Vancouver, British Columbia, Canada. Scenario earthquakes include deep (> 40 km) subducting Juan de Fuca (JdF) plate earthquakes, simulated in locations congruent with known seismicity. Two sets of simulations are performed for a given scenario earthquake using models with and without Georgia basin sediments. The chosen peak motion metric is the geometric mean of the two orthogonal horizontal components of motion. The ratio between predicted peak ground velocity (PGV) for the two simulations is applied here as a quantitative measure of amplification due to 3D basin structure. A total of 10 deep subducting JdF plate earthquakes are simulated within 100 km of Greater Vancouver. Simulations are calibrated using records from the 2001 M_w 6.8 Nisqually earthquake. On average, the predicted level of average PGV at stiff soil sites across Greater Vancouver for an M_w 6.8 JdF plate earthquake is 3.2 cm/s (modified Mercalli intensity IV–V). The average increase in PGV due to basin structure across Greater Vancouver is 3.1. Focusing of north-northeast-propagating surface waves by shallow (< 1 km) basin structure increases ground motion in a localized region of south Greater Vancouver; hence, scenario JdF plate earthquakes located ≥ 80 km south-southwest of Vancouver are potentially the most hazardous.

Online Material: Depth slices of 3D velocity model, peak ground velocity maps, and snapshots and videos of wave propagation.

Introduction

It is well known that earthquake waves are altered by 3D basin structure by the generation of long-period surface waves from the conversion of incident shear waves at the basin edge and/or walls (e.g., Bard and Bouchon, 1980) and by the trapping/focusing of shear waves at the basin edge (e.g., Graves *et al.*, 1998). As an example, long-period (~2 s) earthquake ground motion in the soft clay basin of Mexico City during the 1985 M_S 8.1 Michoacán earthquake, more than 300 km distant, was ~14 times higher (Singh *et al.*, 1988) and lasted nearly three times longer than on firm ground nearby (Roullé and Chávez-García, 2006). Large amplification in sedimentary basins may also result from constructive interference of upward propagating shear waves and laterally propagating surfaces waves from the basin edges, known as the basin-edge effect. For example, the narrow 30 km long damage pattern in Kobe, Japan, is offset ~1 km from the fault plane of the 1995 M_w 6.9 Hyogo-ken-Nanbu earthquake and is attributed to the basin-edge effect (Kawase, 1996; Pitarka *et al.*, 1997).

Finite-difference (FD) modeling of 3D wave propagation for a variety of basins worldwide has generally shown the largest ground motions are predicted to occur near the source, above the deepest part of the basin, and near its steepest-dipping edges (e.g. Frankel and Vidale, 1992; Frankel, 1993; Olsen *et al.*, 1995; Olsen and Archuleta, 1996). Amplification may also occur immediately behind convex basin edges or bottoms as a focusing effect (Olsen and Schuster, 1994; Olsen, 2000a). Simulations of 1D and 2D ground motion generally underpredict duration of generated surface

*Also at Natural Resources Canada, P.O. Box 6000, Sidney, British Columbia V8L 4B2; and now at Department of Civil Engineering, University of British Columbia, 6250 Applied Science Lane, Vancouver, British Columbia V6K 1C1; semolnar@mail.ubc.ca.

†Also at School of Earth and Ocean Sciences, University of Victoria, 3800 Finnerty Road, Victoria, British Columbia, V8P 5C2.

waves as out-of-plane wave propagation and 3D mode conversions are not accounted for. Realistic prediction of ground motion in sedimentary basins subject to the threat of future large earthquakes therefore requires 3D modeling. Ultimately, 3D basin effect simulations should be directly incorporated in the generation of probabilistic seismic-hazard maps, as was carried out for Seattle, Washington, by Frankel *et al.* (2007).

Advances made in FD numerical simulation in the last few decades are largely due to significant effort in predicting earthquake ground motion via 3D numerical methods of shallow earthquakes in California. For example, Graves and Pitarka (2004) extend 3D long-period ($\geq$1 s) FD simulations to shorter periods using a stochastic approach to produce broadband synthetics, whereas Furumura *et al.* (2002) employ an FD method combined with a Fourier spectral method to achieve high-parallel performance for large-grid (50 million) 3D simulations. Nonuniform grid FD schemes also improve computational efficiency (e.g., Pitarka, 1999; Liu and Archuleta, 2002). A comparison of predicted ground motions of shallow California earthquakes by a variety of numerical schemes has generally demonstrated consistency, sufficient accuracy, and reliability (Aagaard *et al.*, 2008a,b; Bielak *et al.*, 2010; Hartzell *et al.*, 2011). The largest discrepancies are due to differences between mesh and grid representations of the same velocity model (Bielak *et al.*, 2010). Variability in predicted ground motion in California due to uncertainties in source or velocity models has been examined; Aagaard, Graves, Rodgers, *et al.* (2010) and Aagaard, Graves, Schwartz, *et al.* (2010) found the largest variability in predicted ground motions due to variation in rupture length (magnitude), hypocenter location, and slip distribution of the source process, whereas Hartzell *et al.* (2010) demonstrated that 5%–10% perturbation in a velocity model may result in up to a factor of 1.5–2.2 difference in predicted ground motions at frequencies $\leq$1 Hz. Other studies have explored variation in predicted ground motion due to variation of both source and velocity models or numerical schemes and source models. For example, Graves and Aagaard (2011) demonstrated that the median predicted peak ground motion of 10 FD simulations (five source models and two velocity models) of the M_w 7.2 El Mayor–Cucapah earthquake is in reasonable agreement with observed measurements, whereas Hartzell *et al.* (2011) perform 12 simulations (four different schemes and three different source models) and find the combined model uncertainty and random variability of simulations are in the same range as variability of regional empirical ground-motion datasets. Day *et al.* (2008) simulated ground motions of 60 shallow earthquakes in the Los Angeles (LA) basin to complement the empirical strong-motion dataset for development of the Next Generation Attenuation of ground-motion relations. They propose a generalized predictor of long-period ground motion (geometric mean of both horizontal components) for any sedimentary basin as the depth to either a shear-wave velocity (V_S) of 1.0, 1.5, and 2.5 km/s (i.e., $Z_{1.0}$, $Z_{1.5}$, and $Z_{2.5}$, respectively), with preference of $Z_{1.5}$ for the LA basin.

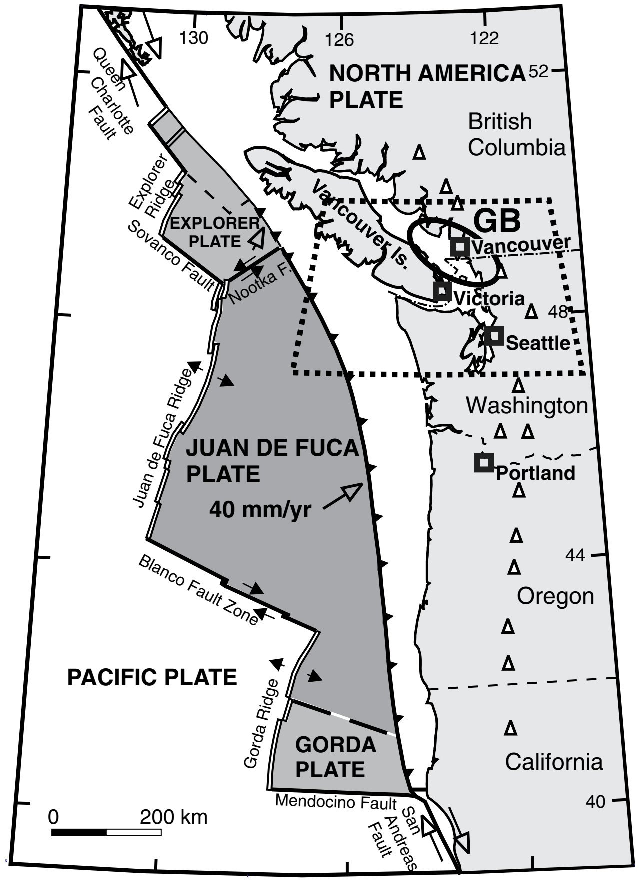

Figure 1. Tectonics of the Cascadia subduction zone (adapted from Hyndman *et al.*, 1996); volcanic centers are shown as triangles. Locations of major cities marked by small boxes and labeled by name, and the international border is marked by a dashed-dotted line. The approximate boundary of the Late Cretaceous Georgia basin (GB) is shown by a thick ellipse. The dotted box corresponds to the limits of the map in Figure 2.

The area of highest seismic risk in Canada is metropolitan Greater Vancouver in southwest British Columbia, with a population exceeding 2 million and critical infrastructure situated above the seismically active Cascadia subduction zone (Onur *et al.*, 2005). In this convergent tectonic setting (Fig. 1), the oceanic Juan de Fuca (JdF) plate subducts in a northeast direction beneath the continental North America plate. Earthquakes occur in three zones: (1) the thrust fault interface between the two plates, which is currently locked and is accumulating strain to be released in future great earthquakes; (2) within the overriding North America plate, which is in compression and results in crustal earthquakes; and (3) earthquakes occur within the subducting JdF plate, mainly in response to bending of the plate at depth. The most frequent earthquakes in Greater Vancouver are JdF plate events (Halchuk and Adams, 2004); the activity rate of M_w 5 JdF plate events per year is determined to be 0.0932 (one every ~10 years), and the best-estimate maximum magnitude is 7.1 (Adams and Halchuk, 2003). Figure 2 shows subducting JdF plate earthquakes are concentrated in Puget

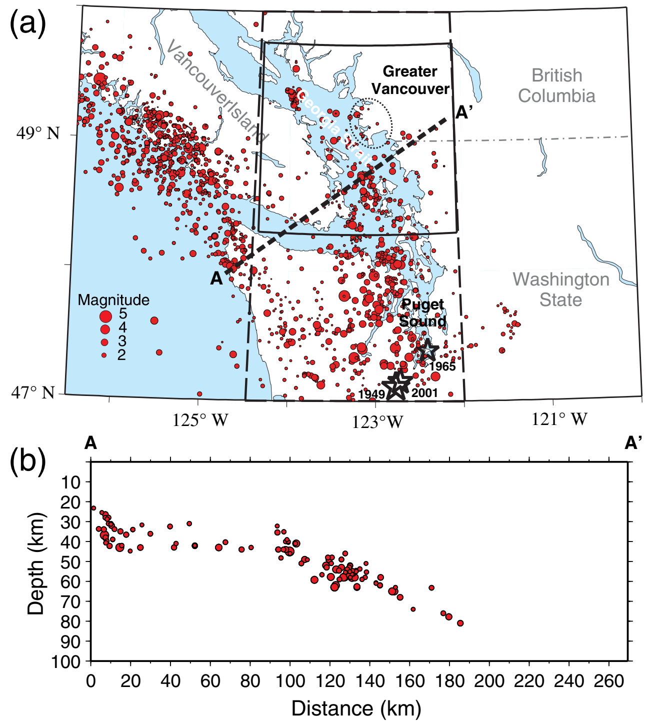

Figure 2. (a) Juan de Fuca (JdF) plate seismicity (1985–1999). Significant earthquakes ($M_w > 6$) are represented by stars and labeled by year. Limits of the Georgia basin regional model are shown by the solid box, and the Pacific Northwest model is shown by the dashed box. The dashed-dotted line is the international border, and the Greater Vancouver region is bounded by the dotted ellipse. The thick dashed line denotes the seismic cross-section A–A$'$, shown in (b) (M_L 2 minimum). The color version of this figure is available only in the electronic edition.

Sound or along Georgia Strait coincident with the bend in the coastline (Rogers, 1998; Bolton, 2003). Events that occur beneath the west coast of Vancouver Island are not of concern to this study. The JdF plate is dipping at a maximum of 30° beneath Georgia Strait and Puget Sound such that the majority of events occur at 45–65 km depth and few extend to 80 km (Bolton, 2003). The larger magnitude JdF plate events tend to exhibit normal faulting (Bolton, 2003; Ristau *et al.*, 2007). The largest JdF plate earthquakes occurred in 1949 (M_w 7.1), 1965 (M_w 6.5), and 2001 (M_w 6.8) beneath southern Puget Sound, whereas a moderate sized event (M_w 5.3) occurred in 1976 beneath Georgia Strait.

Much critical infrastructure in British Columbia, including Canada's second busiest airport, the fourth largest tonnage port in North America, key electrical transmission corridors, and a major ferry terminal, is located on the Fraser River delta in south Greater Vancouver. This area is underlain primarily by Holocene silts and sands and Pleistocene glacial deposits that overlie an irregular Tertiary clastic sedimentary rock surface. This entire sedimentary sequence infills the Georgia basin, a northwest-oriented Late Cretaceous structural depression (Mustard, 1994; England and Bustin, 1998; Hannigan *et al.*, 2001) that extends predominantly east across Georgia Strait to mid-Vancouver Island and south into mainland Washington (Fig. 1). The Georgia basin is one in a series of basins spanning from California to south Alaska along the Pacific margin of North America (England and Bustin, 1998), and is relatively wide and shallow (Tertiary dimensions of 130 by 70 by 5 km) in comparison to basins southward in Seattle (75 by 30 by 8 km; Frankel *et al.*, 2007) and Los Angeles (50 by 30 by 5 km; Magistrale *et al.*, 1996). Properties of the Late Cretaceous and Tertiary sedimentary rocks within the Georgia basin and its basement are known from seismic surveys (e.g., White and Clowes, 1984), particularly seismic tomography results of the 1998 Seismic Hazards Investigations in Puget Sound experiment (Zelt *et al.*, 2001; Ramachandran *et al.*, 2004; Dash *et al.*, 2007).

Amplification of earthquake ground motion in Greater Vancouver from inevitable future large earthquakes not only depends on the 1D soil column and nonlinear response of the near-surface sediments, but also depends on the 3D structure of the Georgia basin. Realistic estimates of earthquake ground motion must account for all of these components. Previous 1D and 2D numerical modeling of earthquake response on the Fraser delta has concentrated on the effect of the relatively shallow soil layering: 1D analyses are based on vertical propagation of *SH* waves upward through a modeled column of the soil layering (thicknesses of investigated sites are 235 m in Molnar, 2011; 300–700 m in Onur *et al.*, 2004; unknown in Finn *et al.*, 2003; and 500 and 700 m in Harris *et al.*, 1998), and the 2D analysis is based on a cross section (30 km north–south extent of 100 m depth) of the Fraser River delta (Finn *et al.*, 2003). Predicted amplification occurs at 0.2–0.4 Hz (first higher-order modes at 1.0–1.5 Hz) due to variable accumulations of Holocene deltaic and/or Pleistocene glacial sequences. Potential amplification due to the relatively deep (upper few kilometers) Georgia basin sedimentary structure is virtually unknown; Tertiary/Late Cretaceous basin sediments are considered as basement in the previous 1D and 2D numerical analyses, and empirical amplification at long periods ($\geq$0.5 Hz) is not resolved by the current strong-motion database, which consists of low-level ($\leq$5%*g*) earthquake recordings of primarily short (~30 s) duration. Amplification observed from these low-level earthquake recordings (0.5 Hz minimum) is 4–11 times that of hard rock at 1.5–4.0 Hz (Cassidy and Rogers, 1999, 2004). Hence, this study uses 3D numerical modeling to address the gap in knowledge of potential long-period amplification due to the relatively deep Georgia basin in southwest British Columbia. In Greater Vancouver, long-period amplification is of concern; for example, over 700 commercial and residential buildings are 12 stories or taller, which are likely to have low-resonance frequencies ($\leq$0.5 Hz).

Sedimentary basins in subduction zone settings similar to the Georgia basin include those in Japan, Taiwan, and Mexico. Iwaki and Iwata (2010) perform long-period (> 3 s) FD simulation of an M_{JMA} 6.5 aftershock to assess applicability of a 3D Osaka basin model. The simulation reproduces the observed peak motion at many stations, but overestimates at some stations, as well as reproduces the empirical horizontal-to-vertical spectral ratio peak period within 1 s at many stations. The Yufutsu basin in Northern Japan generally deepens west to east, with an internal sub-basin that deepens east to west; Aoi *et al.* (2008) perform a series of long-period (> 3 s) FD simulations of the 2003 M_w 8.3 Tokachi-Oki earthquake (42 km depth) with or without particular basin layers and demonstrate that the sub-basin is effective in amplifying and extending long-period motions causing significant damage to oil tanks due to sloshing. Long-period (> 1 s) FD simulations of a small earthquake close to the Taipei basin, Taiwan, by Miksat *et al.* (2010) demonstrates amplification is a factor of 4 (compared to hard rock conditions) due to basin structure; maximum amplification is a factor of 8 once amplification due to the low-velocity Songshan formation is included, which is in fair agreement with observed amplification greater than a factor of 5. Lee *et al.* (2008) demonstrate that the low-velocity Songshan formation dominates the amplification and wave propagation behavior (≤3 Hz resolution) for a simple point source at 1 km depth in a shallow Taipei basin model. High-resolution (20 m grid) spectral element numerical simulations, which include the mountainous topography (≤3 km above sea level) that surrounds the Taipei basin, demonstrate that peak ground motions increase up to 50% in the basin for deep scenario events due to scattering of body waves by the enclosing mountains, which then propagate as surface waves into the basin, whereas for shallow earthquakes, topography scatters surfaces waves and reduces predicted peak motions (Lee *et al.*, 2009). Furumura and Singh (2002) perform spectral-element simulations of both a shallow (17 km) M_w 7.3 interplate earthquake along the Mexican subduction zone and a deep (40 km) M_w 7.5 inslab normal-faulting earthquake in the subducted Cocos plate. The shallow interplate event causes very large ground motions (frequency bandwidth of 0.2–4 Hz) along the path from the coast to the Mexican interior due to interference of multiple crustal arrivals (*Lg* phase), whereas ground motions for the deeper inslab normal-faulting event demonstrate simple attenuation with increasing distance, that is, the *Lg* phase is too small.

This paper presents FD simulations of long-period (> 2 s) ground motions computed for scenario deep JdF plate earthquakes in southwest British Columbia in a regional 3D velocity model of the Georgia basin, Molnar *et al.* (2014) deals with shallow (5 km) crustal North America plate scenario earthquakes (Molnar *et al.*, 2014). This research provides the first detailed investigation of 3D earthquake ground motion for a sedimentary basin in Canada. The main objective here is to examine the effect of the 3D Georgia basin structure on predicted ground shaking across Greater Vancouver from large (M_w 6.8) scenario earthquakes. The scenario earthquakes considered in this paper include deep (42–55 km) subducting JdF plate events with a seismic radiation pattern equivalent to that of the normal-faulting 2001 M_w 6.8 Nisqually, Washington, earthquake. Scenario earthquakes are simulated in different epicenter locations in the Georgia basin region, congruent with known seismicity and within 100 km of Vancouver, to investigate variation in the strength of predicted ground motions and 3D basin effects. The chosen peak ground velocity (PGV) metric here is geometric mean of the two orthogonal horizontal components, calculated as $\max_t(\sqrt{v_{EW}(t) \times v_{NS}(t)})$, in which $v(t)$ represents a synthetic horizontal velocity waveform, EW represents east–west component and NS represents north–south component. The preferred intensity measure of the American Society of Civil Engineers (ASCE) has changed from the geometric mean value (ASCE, 2006) to the maximum rotated value (ASCE, 2010) of the two orthogonal horizontal components. Peak motion values based on the square-root sum of squares of both horizontal and all three components of motion, termed 2DrssPGV and 3DrssPGV, respectively, are also provided here as an approximation of maximum rotated PGV (NEHRP Consultants Joint Venture, 2011). Amplification due to basin structure is evaluated as the ratio of peak motion from simulations of the same scenario earthquake in 3D basin and nonbasin structure models, as performed for the LA basin by Olsen (2000b). In order to conduct this research, the Georgia basin 3D structure model is revised with recent geological and geophysical information and calibrated by simulating the Nisqually earthquake and comparing the synthetic results to recordings. Limitations of this work include: (1) uncertainty in physical-structure and source-rupture models, (2) omission of low-velocity material (e.g., water and up to 300 m of Holocene sediments) and surface topography in the physical-structure models, and (3) inability to resolve frequencies > 0.5 Hz. Nonetheless, the work presented here (and in Molner *et al.*, 2014) represents an important first step toward quantifying the effect of the 3D sedimentary Georgia basin structure on earthquake ground motion in southwest British Columbia.

Physical-Structure Models

The base elastic 3D model is extracted from the Stephenson (2007) Pacific Northwest 3D velocity model that was produced for simulations of M_w 9 Cascadia megathrust events (Olsen *et al.*, 2008). Two different sizes of physical-structure models are used; a Pacific Northwest model that spans from northwest Washington to southwest British Columbia (dashed box in Fig. 2) is used for simulation of the Nisqually earthquake at > 150 km from Greater Vancouver, and a smaller regional model (solid box in Fig. 2) is used for simulations of scenario JdF plate earthquakes within 100 km of Greater Vancouver. Table 1 provides details of the Pacific Northwest and regional velocity models.

The physical-structure model is described fully in Stephenson (2007) and only a brief overview is given here. The physical model is represented by six geologic units (continental basin sediments, crust, and mantle; and oceanic sediments, crust, and mantle) characterized by V_P, V_S, and density. The thickness of the oceanic crust was set to 5 km. The 3D sedimentary basin structure in the Georgia basin

Table 1
3D Modeling Parameters

Parameter	Regional Model*	Pacific Northwest model†
Spatial discretization	250 m	250 m
Temporal discretization	0.014 s	0.014 s
Lowest V_P	1562.5 m/s	1500 m/s
Lowest V_S	625 m/s	0 m/s
Lowest ρ	1674 kg/m^3	1025 kg/m^3
Number of grid nodes (extent) in x direction	720 (180 km)	1350 (337.5 km)
Number of grid nodes (extent) in y direction	600 (150 km)	800 (200 km)
Number of grid nodes (extent) in z direction	240 (60 km)	240 (60 km)
Number of time steps (simulation duration)	5000 (70 s)	8571 (120 s)
Numerical averaging	Harmonic	Arithmetic
Boundary conditions	Perfectly-matched absorbing layers	Cerjan
Wall clock time	~7 hours	~72 hours

*Used for simulation of 10 deep JdF plate scenario earthquakes within 100 km of Greater Vancouver.

†Used for simulation of the Nisqually earthquake at > 150 km distance from Greater Vancouver.

region is primarily constrained by the tomographic V_P model (1 km resolution) of Ramachandran *et al.* (2004, 2006). The V_P/V_S ratio for Quaternary basin sediments varies from 2.5 at the surface to 2.2 at 1 km depth. Tertiary sediments are set to a V_P/V_S ratio of 2, and their base is taken as the 4.5 km/s V_P contour (Ramachandran *et al.*, 2006). Densities are derived from the V_P model using the Nafe–Drake relation (Ludwig *et al.*, 1970). Surface topography is not included. The minimum V_S is set to 625 m/s for computational feasibility (Olsen *et al.*, 2008). In south Greater Vancouver, up to 300 m of Holocene deltaic sediments of the Fraser River are effectively ignored, that is, are represented by a V_S of 625 m/s. The surface of the 3D basin model therefore represents overconsolidated Pleistocene glacial sediments or stiff soil sites. This is a significant limitation to modeling of the potential earthquake ground motion here, and the overall amplitude and duration of simulated ground motions in the Georgia basin are likely biased. For example, if > 200 m of lower-velocity material is present, applicable to the Fraser River delta in south Greater Vancouver, amplification will be increased by a factor of ~2 from that presented here (Molnar, 2011).

For the FD simulations carried out in this paper (in Molner *et al.*, 2014), the upper 1 km of the base elastic 3D model is updated in the Georgia basin region of southwest British Columbia. Regions with thick accumulations of unconsolidated Pleistocene and younger sediments known from high-resolution shallow seismic data (Hamilton, 1991; Mosher and Hamilton, 1998) are not resolved in regional tomographic V_P models (Lowe *et al.*, 2003). In the base elastic 3D model, a northeast-trending velocity contrast occurs beneath Greater Vancouver, which is not supported by geological and structural information, but rather results from extrapolation of the 1 km gridded V_P model of Ramachandran *et al.* (2006) to the surface. When the base elastic 3D model is used in FD simulations of the Nisqually earthquake, good agreement is obtained between synthetic and empirical waveforms in the Seattle basin region (Molnar *et al.*, 2010), because significant effort had gone into validating the 3D model (Frankel and Stephenson, 2000; Hartzell *et al.*, 2002; Pitarka *et al.*, 2004; Frankel *et al.*, 2007, 2009). However, synthetic waveforms overpredict Nisqually waveform amplitudes in the Georgia basin region by a factor of 2.1 (Molnar *et al.*, 2010). Therefore, in order to update V_P in the upper 1 km of the base elastic 3D model in the Georgia basin region for the modeling work conducted here, all nonconfidential government geological and geophysical datasets, as well as the higher-resolution (600 m gridded) tomographic regional model of Dash *et al.* (2007), were collected, converted to V_P estimates (if required), and merged (details in Molnar, 2011). The V_P/V_S ratio is set to 2 for $V_P \leq 5.5$ km/s in the updated 3D basin model; the base of the Georgia basin is composed of Late Cretaceous Nanaimo Group rocks, inferred as the 5.5–6.0 km/s V_P surface in regional tomographic V_P models (Zelt *et al.*, 2001; Ramachandran *et al.*, 2004, 2006; Dash *et al.*, 2007). This higher V_P limit for the V_P/V_S ratio of 2 effectively causes low V_S values to extend to greater depths in the updated model. Otherwise, relationships of V_P with V_S remain unchanged. Densities are derived from the V_P model using the Nafe–Drake relation (Ludwig *et al.*, 1970) and are in agreement with the 3D Georgia basin density model of Lowe *et al.*, (2003).

A nonbasin 3D model is also generated from the updated basin model by setting the minimum V_P to 5.5 km/s, effectively replacing basin sediments with inferred basement. Structural studies in this region have shown that basement units surrounding the Late Cretaceous Georgia basin sediments correspond to V_P of ~5.5–6.0 km/s in the upper 2 km and ~6.4–6.75 km/s at deeper depths (White and Clowes, 1984; Zelt *et al.*, 2001; Ramachandran *et al.*, 2004, 2006; Dash *et al.*, 2007). Expected reduction in seismic velocity of basement rock units in southwest British Columbia likely occurs in the upper tens of meters, which is not resolved by the chosen 250 m gridded velocity model. Therefore, the nonbasin velocity model is based on the typical 1D velocity profile for rock sites in southwest British Columbia. Figure 3 compares the 500 m depth surface and 8 km deep cross sections of the updated basin and nonbasin regional models (see Ⓔ Fig. S1 for depth surfaces to 7 km, available in the electronic supplement to this paper). The maximum depth of the Georgia basin is 6.5 km at its southeast extent; hence, the basin and nonbasin models are identical below 6.5 km depth. Simulations using the nonbasin model represent shaking due to source characteristics and background regional structure. For the same scenario earthquake, the ratio of peak motions predicted using the basin and nonbasin models provide a quantitative measure of 3D Georgia basin effects. The advantage of

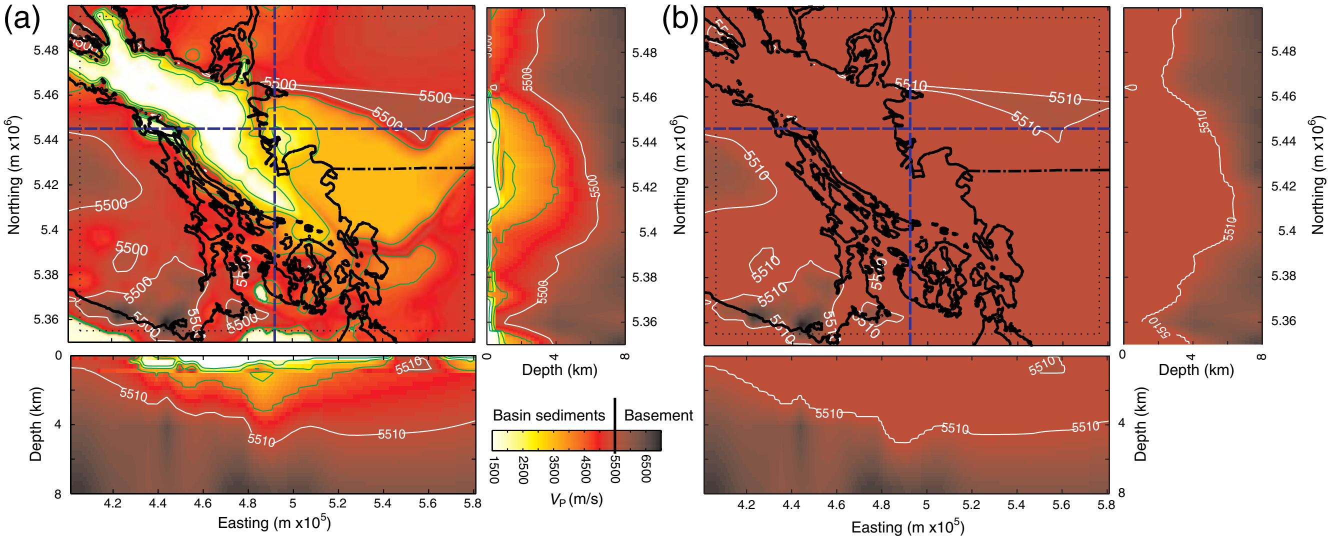

Figure 3. Depth slices at 500 m of the updated (a) basin and (b) nonbasin regional V_P models (coastline is the thick black line). The dashed-dotted line is the international border, and the dotted box denotes the 5 km boundary zone. Thick dashed lines correspond to east–west and north–south vertical cross sections of each model, shown in the panels below and to the right, respectively (only the upper 8 km of the full 60 km depth model is shown). In all panels, thin lines correspond to the contours of V_P at 1500, 2500, 3500, and 4500 m/s, and the thin white line is $V_P \sim 5500$ m/s. Ⓔ Figure S1, available in the electronic supplement to this paper, shows select depth slices of basin and nonbasin models to 7 km depth. The color version of this figure is available only in the electronic edition.

calculating basin/nonbasin ratios of peak motion noted by Olsen (2000b) is the removal of geometrical spreading effects included in the basin response and the nonbasin reference value for a given site, with the disadvantage that artifacts occur in maps of basin/nonbasin peak motion due to singularities in the rupture pattern.

Finite-Difference Scheme

The 3D elastic equations of motion are solved here using the FD scheme of Olsen (1994) with fourth-order accuracy in space and second-order accuracy in time. This scheme has been verified against other FD and finite-element methods for reference (1D) benchmarks as well as realistic basin (3D) shapes (e.g. Day *et al.*, 2008; Bielak *et al.*, 2010). The physical model is represented by a uniform cubic mesh discretized with a spacing equivalent to five nodes per minimum shear wavelength (e.g., Levander, 1988; Moczo *et al.*, 2000), which limits the maximum resolvable frequency. In this work, the uniform grid size of the physical model is 250 m, with a minimum V_S of 625 m/s, such that the maximum resolvable frequency is 0.5 Hz (2 s period). Viscoelasticity is incorporated independently for P and S waves using a coarse-grained implementation of the memory variables (Day, 1998; Day and Bradley, 2001). Generally, the most important parameters for ground-motion prediction are V_S and Q_S, which govern shear and surface-wave arrivals associated with the strongest ground motions (Brocher, 2007). Various Q relations were tested (Olsen, 2003; Brocher, 2008; Frankel *et al.*, 2009) but cause minimal variation to the resulting low-frequency ground motions. The Q relations of Frankel *et al.* (2009) for stiff sediments in the Pacific Northwest are the most geologically reasonable and are assigned here: for $V_S <$ 1000 m/s, $Q_S = 0.1643 \times V_S - 14$; for $V_S > 1000$ m/s, $Q_S = 0.15 \times V_S$; and $Q_P = 2 \times Q_S$. Overall, Q_S increases from 89 at the surface to 723 at 60 km depth in the updated 3D basin model.

Table 1 provides further details of the modeling parameters. The FD code was compiled on the Minerva IBM Nighthawk-2 SP supercomputer at the University of Victoria. The Nisqually earthquake is simulated using arithmetic averaging (Olsen, 1994; version 2.5.1) and absorbing boundary conditions (Clayton and Engquist, 1977) including a zone of highly attenuative material (Cerjan *et al.*, 1985) in the Pacific Northwest model (2.6×10^8 grid nodes). For this model, the use of the generally higher-accuracy harmonic averaging is inhibited by the presence of water in the model with $V_S = 0$. All other deep JdF plate events are simulated within 100 km of Greater Vancouver using harmonic averaging (Olsen, 1994; version 2.6.4) and more efficient perfectly matched absorbing layers boundary conditions (Collino and Tsogka, 2001; Marcinkovich and Olsen, 2003) in the Georgia basin region model (1.0×10^8 grid nodes). The seismic source is implemented in the FD grid by adding $-M_{ij}(t)/V$ to $S_{ij}(t)$, in which $M_{ij}(t)$ is the ijth component of the moment tensor for the earthquake, $V = dx^3$ is the cell volume, and $S_{ij}(t)$ is the ijth component of the stress tensor on the fault at time t (Olsen, 2000b).

Earthquake Source Model

The most recent and best-constrained large magnitude earthquake in the Pacific Northwest is the 2001 M_w 6.8 Nisqually earthquake. Of the 12 earthquakes recorded since

Table 2
Details of Nisqually Earthquake Source Model

Point Source	Strike (°)	Dip (°)	Rake	Rise Time (s)	Seismic Moment (N·m)
1	356°	68°	−90°	4.0	0.7×10^{19}
2	356°	68°	−100°	4.5	1.1×10^{19}

Latitude is 47.15° N, longitude is −122.73° E, and depth is 55 km.

the 1960s by the strong-motion network in southwest British Columbia (Cassidy *et al.*, 2008), the Nisqually earthquake generated the highest-quality dataset with 96 recordings of 15–90 s recording length and sufficient signal-to-noise ratio. From seven studies of the Nisqually earthquake's source parameters (Bustin *et al.*, 2004), the earthquake is a normal-faulting event that ruptured at 49–55 km depth along a north-striking, steeply east-dipping fault (or south-striking shallow west-dipping fault) and released a total seismic moment of $1.4–2.0 \times 10^{19}$ N·m. Kao *et al.* (2008) applied a source-scanning algorithm to local seismic waveforms and showed unambiguously that rupture occurred along the north-striking steeply east-dipping fault plane. The imaged source process occurs in two pulses, with a slightly stronger second pulse and a total duration of ∼6–7 s. Rupture characteristics of other large JdF plate events in 1949 and 1965 are also best represented by a double-pulse release of seismic moment (Ichinose *et al.*, 2004, 2006; Wiest *et al.*, 2007), with a duration of 12–22 s for the larger (M_w 7.1) 1949 event (Wiest *et al.*, 2007). Hence, a source model based on the Nisqually earthquake rupture is considered to best represent rupture for large JdF plate earthquakes and is used here for all 10 scenarios.

Previous FD simulations of the Nisqually earthquake, including comparison with recordings, for the Seattle basin region were carried out by Pitarka *et al.* (2004) and Frankel *et al.* (2007, 2009). Table 2 provides details of the Nisqually earthquake source model of Pitarka *et al.* (2004), used here for the Nisqually earthquake and all 10 scenario earthquake simulations. This model is also used by Frankel *et al.* (2009), whereas Frankel *et al.* (2007) used a slightly longer duration of 1.7 s between point sources. Variations of the Nisqually earthquake source model were tested for this study: a 50% reduction or 20% increase in PGV (single horizontal component) was observed when the source model was adjusted to release the total seismic moment in a single 8.5 s pulse or in two consecutive 4.0 s pulses, respectively, but negligible PGV variation was observed when the two pulses were separated by 1.5 s or 1.7 s (Molnar *et al.*, 2008).

Accuracy of the Simulations

Finite-difference simulation of the Nisqually earthquake is performed here, using the updated 3D Pacific Northwest basin model to calibrate synthetic results with recordings to more accurately predict long-period ground motions for large JdF plate scenario earthquakes. Figure 4 compares empirical and synthetic waveforms at 18 selected strong-motion sites in the Seattle basin region (generally similar sites chosen by Pitarka *et al.*, 2004, and Frankel *et al.*, 2007, 2009). All empirical waveforms are synchronized to 10:54:26 PST (time zero), the origin time of the Nisqually earthquake is 6.78 s later at 10:54:32.78 PST, and the synthetics have been shifted to 10:54:33.75 PST (i.e., synthetic *S* waves arrive ∼1 s later than empirical). The qualitative agreement observed between waveforms here is similar to that shown in Pitarka *et al.* (2004) and Frankel *et al.* (2007, 2009). The deep Seattle basin structure generates more complex and longer duration synthetic waveforms than at sites outside of the basin. Significant long period ground motions are generated at the south edge of the Seattle basin (strong velocity contrast), in agreement with observed stronger amplification for earthquakes from the south-southwest (Frankel *et al.*, 2009) and coincident with the zone of chimney damage from the Nisqually earthquake (Stephenson *et al.*, 2006).

Figure 5 presents waveform comparisons for 16 selected weak- and strong-motion sites in the Georgia basin region. Of the 16 sites, two are strong-motion stations in northeast Washington, four are weak-motion seismograph stations of the Canadian National Seismograph Network located on rock sites surrounding the Georgia basin, and the remaining 10 stations are strong-motion stations of the Geological Survey of Canada and British Columbia Hydro located in Greater Vancouver, four of which are located on low-velocity Holocene sediments of the Fraser River delta (not included in the 3D basin model). The duration of earthquake recordings at rock sites is generally <35 s; longer duration records of 50–97 s are obtained at the soil sites. These strong-motion instruments operate on batteries with internal clocks that drift over time, such that accurate timing is not obtained. Each empirical waveform is shifted based on best visual fit with the corresponding synthetic waveform, the average offset is ∼55 s, similar to the time of the *S*-wave arrival at weak-motion seismograph sites with accurate timing (i.e., ∼50 s at SNB and ∼60 s at HNB).

Ground motions in the Georgia basin region from the M_w 6.8 Nisqually earthquake are significantly lower than in the Seattle basin region, as the deep earthquake is >150 km distant. Recordings at stations south of the Georgia basin (ERW, PGC, SBES, and SNB) generally show larger east–west than north–south arrivals (Fig. 5), in agreement with predictions, but overall the predicted amplitudes are larger. For stations in the Georgia basin (ANN, ARN, EBT, ING, KID, and RHA), predicted PGV is associated with later arriving surface waves, east–west motion is larger than north–south motion, and there is generally good agreement with recordings. Good peak agreement occurs because empirical PGV at soil sites (ANN, ARN, KID, and RHA) is similar to the PGV of later arriving surface waves in the synthetic waveforms.

Following Frankel *et al.* (2009), Figure 6 compares empirical and predicted PGVs for all 36 selected recording sites in Washington and British Columbia. All waveforms are

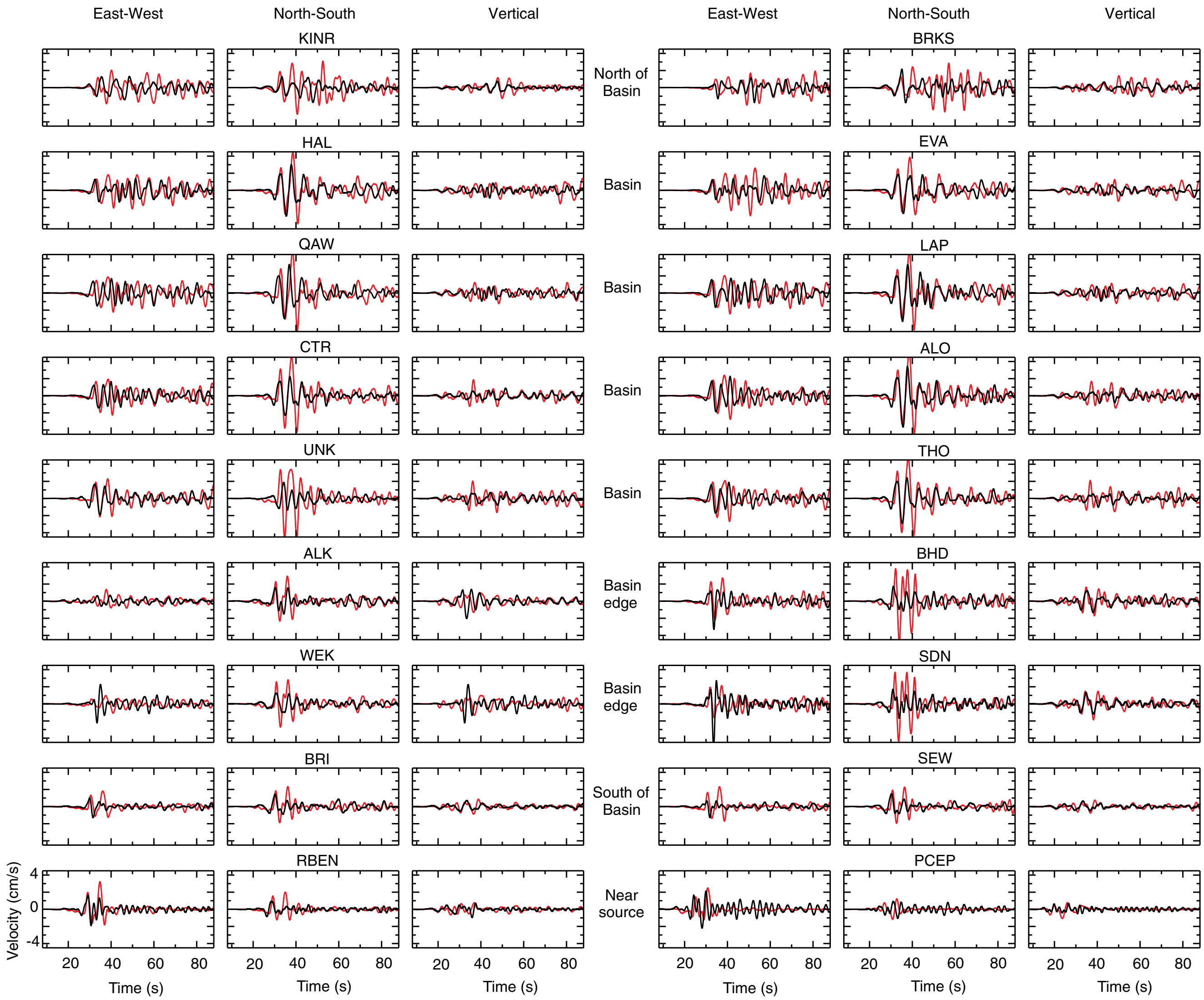

Figure 4. Comparison of 0.01–0.5 Hz synthetic (light lines) and empirical (black lines) long-period Nisqually earthquake waveforms at 18 stiff-soil and/or rock sites in the Seattle basin region, Washington. The color version of this figure is available only in the electronic edition.

band-pass filtered between 0.01 and 0.5 Hz. The simulations conducted in this study generally overpredict empirical PGVs in the Seattle basin region (PGV $>$ 1 cm/s) but capture the trend of the data. For the 18 sites in the Seattle basin region, the bias in PGV is 0.44 natural log units (factor of 1.5; synthetics larger than recorded) with one standard deviation of 0.35 natural log units (factor of 1.4). In comparison, goodness-of-fit factors in peak motion within the Seattle basin region obtained by Pitarka *et al.* (2004) are similar to this study (Molnar, 2011). Frankel *et al.* (2009) use the same physical-structure and source-rupture models as used here to simulate the Nisqually earthquake but use a nonuniform FD scheme. They report a PGV bias of 0.096 natural log units (factor of 1.1) with one standard deviation of 0.27 natural log units (factor of 1.3), band-pass filtered between 0.2 and 0.4 Hz, for 12 sites in the Seattle basin region. If the same filter bandwidth is applied here for the same 12 Seattle basin sites, the 2DgmPGV bias is then 0.30 natural log units (factor of 1.3) and one standard deviation of 0.28 natural log units (factor of 1.3).

Figure 6 shows larger variation is obtained between empirical and predicted PGVs in the Georgia basin region (PGV $<$ 1 cm/s). The average factor of PGV overprediction in the Georgia basin region is 2.1 for the Stephenson (2007) velocity model (6a) and 1.6 for the updated velocity model (6b); incorporation of high-resolution shallow seismic data in the basin velocity model results in an average 24% reduction in bias of predicted PGV.

Simulation of the M_w 6.8 Nisqually earthquake and comparison with recordings demonstrates good agreement in amplitude and phase of first arrival *S* waves at stations within 100 km of the source (Seattle basin region, Fig. 4), providing confidence in the Nisqually source model. Overall, general agreement of the waveforms in the Seattle basin region is

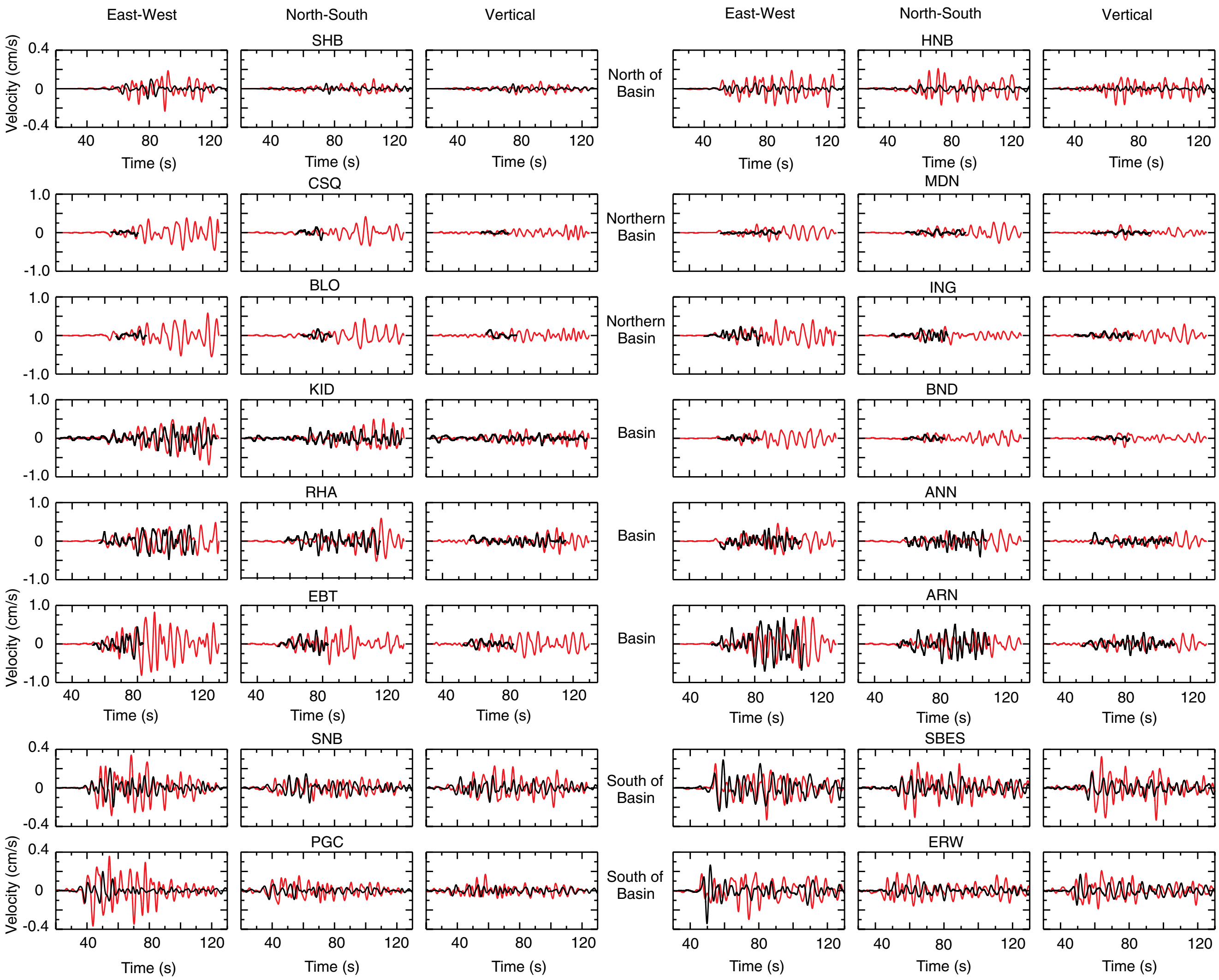

Figure 5. Comparison of 0.01–0.5 Hz synthetic (light lines) and empirical (black lines) long-period Nisqually earthquake waveforms at 16 sites in the Georgia basin region, spanning north Washington to southwest British Columbia. The color version of this figure is available only in the electronic edition.

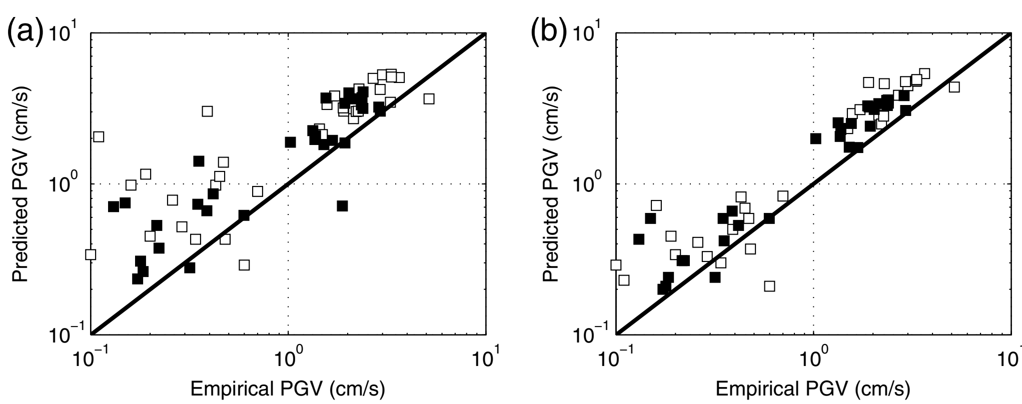

Figure 6. Comparison of predicted and empirical PGVs for the Nisqually earthquake from 3D FD simulations using (a) the Stephenson (2007) velocity model and (b) the updated basin velocity model. Open squares are based on the largest 0.01–0.5 Hz peak velocity from the two horizontal components for a given station; filled squares are based on the geometric mean of the two horizontal components at a given site.

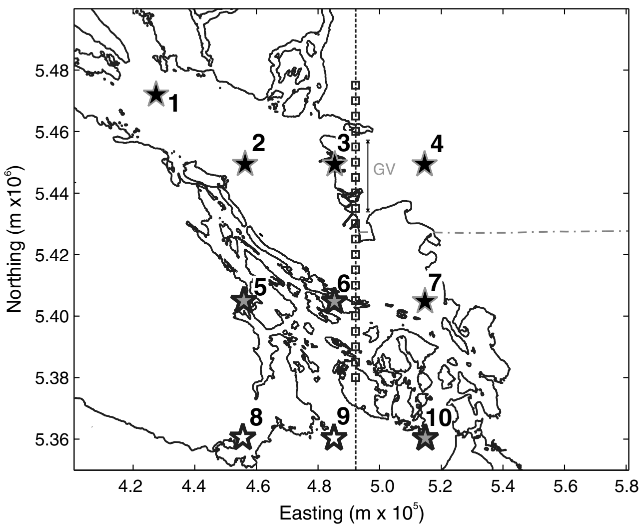

Figure 7. The 10 scenario earthquake epicenter locations are shown by stars (fill corresponds to hypocenter depth: white, 42 km; gray, 48–53 km; and black, 55 km). The coastline is indicated by the black line and international border by the dashed-dotted gray line. Squares along the north–south cross section correspond to the 20 locations of extracted seismograms (5 km spacing) shown in Figure 10, and 5 locations spanning Greater Vancouver (GV) are marked by the dashed vertical line.

achieved, and estimates of PGV are overpredicted by a factor of ~1.5. For the Georgia basin region, validation of the simulated ground motions with generally low amplitude and short duration recordings of the Nisqually earthquake is a challenge, especially without accurate timing for a majority of the recordings and knowledge that the waves propagating north out of the Seattle basin region are already slightly overpredicted before they enter the Georgia basin from the south. However, the Nisqually source model is shown to provide reasonable agreement in the near-source region, such that simulations of large JdF plate scenario earthquakes in the Georgia basin region are conducted using this source model.

Table 3
Location of Each Scenario Earthquake Hypocenter

Scenario	Easting (m)*	Northing (m)*	Approximate Latitude (° N)	Approximate Longitude (° W)	Depth (km)
1	427700	5472300	49.4	124.0	55
2	456450	5449800	49.2	123.6	55
3	485450	5449800	49.2	123.2	55
4	514950	5449800	49.2	122.8	55
5	456450	5405300	48.8	123.6	48
6	485450	5405300	48.8	123.2	53
7	514950	5405300	48.8	122.8	55
8	466450	5361050	48.4	123.5	42
9	485450	5361050	48.4	123.2	42
10	514950	5361050	48.4	122.8	49

*Universal Transverse Mercator coordinates, WGS 1984, Zone 10.

Scenario Earthquakes

The goal here is to quantify the 3D Georgia basin effect on long-period ground shaking in Greater Vancouver for realistic scenarios of M_w 6.8 JdF plate earthquakes. Figure 7 shows the epicenter locations of 10 scenario JdF plate earthquakes considered here, chosen in a 30–40 km grid-spacing spanning the Georgia basin region congruent with known seismicity (Fig. 2). At each scenario earthquake location (Table 3), the Nisqually earthquake source model is initiated near the top of the oceanic crust which subducts northeast beneath Greater Vancouver; hence, the deepest earthquakes occur toward the northeast. The maximum source depth is constrained to 55 km by the maximum 60 km depth of the regional velocity structure models (Table 1). The most realistic scenarios are those along the extent of the Georgia Strait for the chosen magnitude and depth limitations of the model (scenarios 1, 2, 6, 9, and 10); ground motions are likely biased upward for scenarios furthest northeast (scenarios 3 and 4).

Ground-Motion Modeling

Figure 8 shows time snapshots at 5 s intervals of the east–west component PGV for the 70 s simulation of deep JdF plate earthquakes with epicenter locations 40 km west (scenario 2), 50 km south (scenario 6), and 95 km south (scenario 9) of Greater Vancouver. For time snapshots of all three components of motion, see Ⓔ Figure S2 (available in the electronic supplement); the largest motion occurs on the east–west component due to rupture of the north-striking steeply east-dipping normal-faulting source model. Videos Ⓔ of simulations for these three selected scenario earthquakes are available in the electronic supplement. For all 10 scenario earthquakes, surface ground shaking does not occur until 10–15 s into the simulations due to the 42–55 km source depths. The double-pulse nature of the rupture is evident at 20–25 s as two circular wavefronts radiating outward from the scenario epicenter location. The symmetry of the rupture is distorted as waves enter the Georgia basin, that is, wave motion is slowed down by the presence of lower-velocity basin sediments. From 30 s onward, basin surface waves are generated, primarily aligned in a northwest–southeast sense along the basin axis, and are sustained within the basin. The largest amplitude surface waves are generated offshore of Greater Vancouver, toward the northwest and south, coincident with steep edges in the upper 1 km of the basin model. The largest amplitude surface waves arriving in Greater Vancouver occurs at ~50 s for scenario 8, 100 km southwest of Vancouver from focusing (constructive interference) as they propagate north across the city. Larger amplitude surface waves in Greater Vancouver are not produced by any of the other nine simulated deep JdF plate earthquakes, although multiple cycles of slightly lower-amplitude surface waves at ≥60 s are generated in Greater Vancouver for scenario 9, 95 km south of the city.

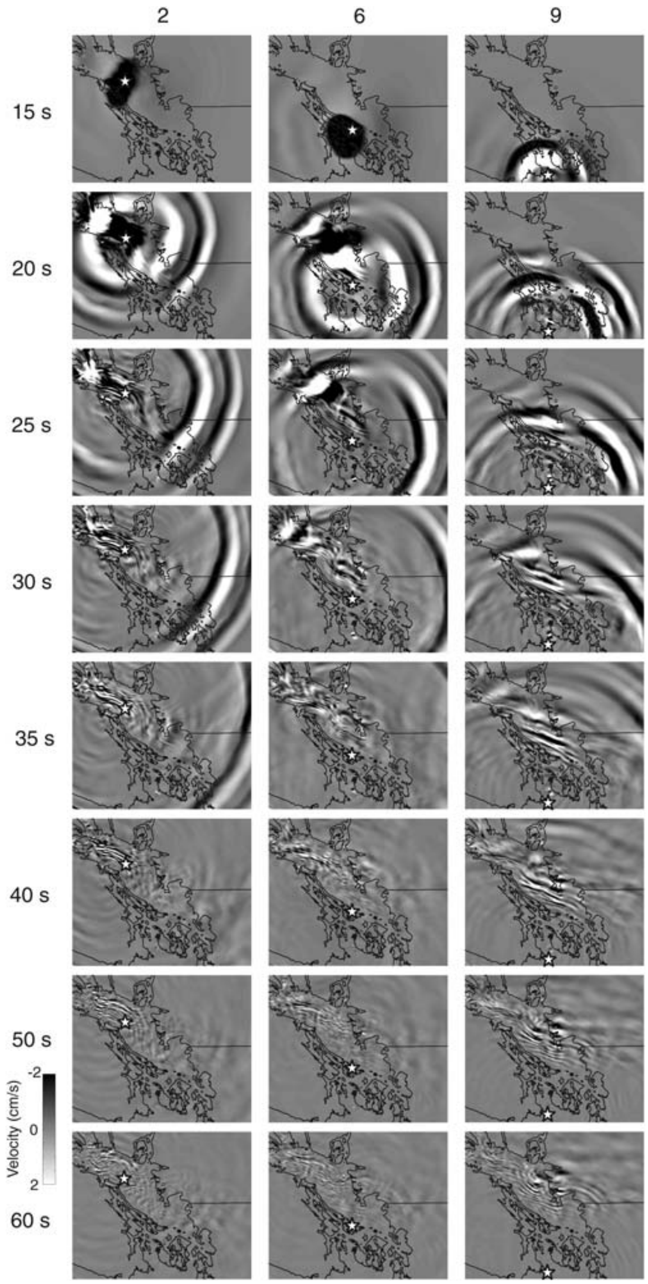

Figure 8. Snapshots of the simulated east–west component wave propagation for scenario earthquakes 2, 6, and 9 (stars show epicenter locations) from 15 to 60 s after the origin time of the rupture; the coastline and the international border are shown as black lines.

Table 4 lists the maximum PGV (three different metrics) within the Georgia basin and Greater Vancouver regions for each scenario earthquake, as well as the average maximum PGV for all 10 scenario earthquakes for each region. The 2DrssPGV values are generally higher than the preferred geometric mean PGV (2DgmPGV) values, as expected, and are similar to 3DrssPGV values because the vertical component motion is here generally of smaller or similar amplitude to horizontal motion here. Figure 9 shows PGV maps (2DgmPGV metric) for all 10 scenarios; panel layout corresponds to the spatial distribution of scenario earthquake epicenter locations. Ⓔ Figures S3 and S4, available in the electronic supplement to this paper, show PGV maps of each individual component of motion and 3DrssPGV, respectively, for all 10 scenarios. Generally, the highest ground motions are coincident with the lowest velocity sediments in the upper 1 km of the model (see Figs. 1 and Ⓔ S1a in the supplement), although the level and spatial extent of ground shaking is unique to each scenario. The range in predicted maximum PGV in the Georgia basin region is 4.8 to 9.1 cm/s, modified Mercalli intensity (MMI) of V–VI (Worden *et al.*, 2012). Maximum PGV in Greater Vancouver ranges from 2.6 to 4.3 cm/s, corresponding to MMI IV–V. For context, the M_w 6.8 Nisqually earthquake produced long-period shaking levels ≤5 cm/s in the Seattle basin (Fig. 4) and resulted in U.S. $2 billion worth of damage in Washington.

Basin Amplification

Figure 10 displays east–west component waveforms at 20 locations along a 100 km long north–south profile (5 km spacing) through Greater Vancouver for 8 selected scenario events simulated in both the basin and nonbasin models. The bottom panels display the cross-sectional velocity structure for each model to 10 km depth (maximum model grid depth is 60 km). Ⓔ Figure S5, available in the electronic supplement, compares basin and nonbasin waveforms for the north–south and vertical components. For each scenario, predicted amplitudes and duration of shaking is increased within the basin (at distances of ~25–75 km) in comparison to nonbasin model simulated waveforms. All waveforms display two early *S*-wave arrivals due to the rupture character of the source. The amplitude of these early *S*-wave arrivals is largest in Greater Vancouver for the deep JdF plate earthquake 25 km east of the city (scenario 4). The largest later-arriving surface waves in Greater Vancouver occur for the scenario 100 km southwest of Greater Vancouver (scenario 8). Figure 10 clearly shows the predicted variation in shaking level and duration for the 10 scenarios of deep JdF plate earthquakes within the Georgia basin region.

Figure 11 shows basin amplification maps (ratio of 2DgmPGV between basin and nonbasin simulations) for the 10 scenario JdF plate earthquakes. As an example, the east–west component waveform at a selected location within Greater Vancouver is also shown in Figure 11 for the basin and nonbasin model simulations of each scenario earthquake. The presence of the northwest-oriented Georgia basin is readily apparent and is associated with amplification factors ≥2.5. The highest basin amplification (up to a factor of 11) generally occurs near each earthquake epicenter but is generally coincident with the lowest-velocity Georgia basin sediments in the upper 1 km (see Figs. 3 and Ⓔ S1a in the supplement). In Greater Vancouver, the highest ground motions are associated with the scenario earthquake 25 km east of the city (scenario 4), but the highest basin amplification

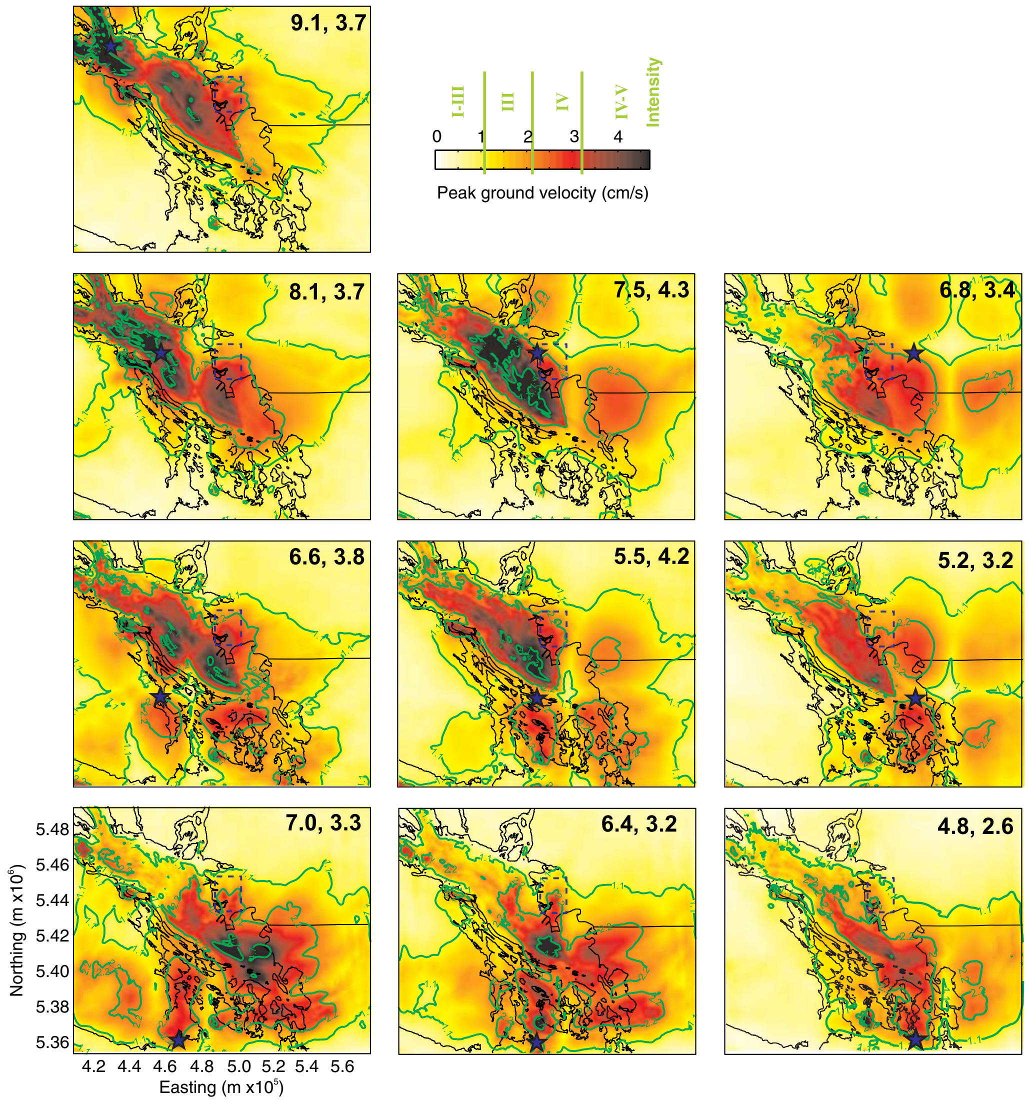

Figure 9. Maps of PGV (cm/s) for all 10 scenario earthquakes (contour lines correspond to the modified Mercalli intensity [MMI] intervals of Worden *et al.*, 2012); stars show the epicenter locations, and coastline and the international border are shown by the black lines. Numbers in the upper right of each panel correspond to maximum PGV within the Georgia basin (map area shown north of 5.38×10^6 m) and Greater Vancouver (dashed rectangle) regions. The color version of this figure is available only in the electronic edition.

(factor of >4.5) is associated with scenario earthquakes located ≥80 km south-southwest of the city (scenarios 8, 9, and 10) due to the occurrence of later-arriving surface waves in basin model waveforms. Basin amplification factors based on the 3DrssPGV metric are listed in Table 4 and Ⓔ displayed in Figure S6 (available in the electronic supplement). Generally, basin amplification factors increase as PGV values decrease; the 3DrssPGV metric determines the highest PGV values and the lowest, and most stable, basin amplification factors.

Discussion

A set of 10 scenario M_w 6.8 JdF plate earthquakes are simulated in the Georgia basin and nonbasin structure models to predict long-period ground motions in Greater Vancouver. Figure 12 presents maps of the average PGV and basin amplification of all 10 scenario earthquakes. These maps are considered to provide an estimate of the average peak motion and basin amplification related to a deep JdF plate earthquake within 100 km of Greater Vancouver. The presence of the Georgia basin significantly increases the level of predicted long-period ground motions. For the Georgia basin region as a whole, the average maximum PGV is 4.6 cm/s, related to an MMI V. The average maximum basin amplification is a factor of 4.5. For comparison, Olsen (2000b) determined the average maximum basin amplification of the LA basin for nine scenario events to be 4.2.

More importantly, in the onshore Greater Vancouver region, the average maximum peak motion is 3.2 cm/s. Therefore, on average, the predicted intensity of shaking at stiff soil sites in Greater Vancouver for an M_w 6.8 JdF plate

Table 4
Maximum PGV (cm/s) and Associated Basin Amplification Factor

Scenario	2DgmPGV* (cm/s)	2DrssPGV† (cm/s)	3DrssPGV‡ (cm/s)	2DgmPGV* (factor)	2DrssPGV† (factor)	3DrssPGV‡ (factor)
Georgia Basin Region						
1	9.1	14.7	15.3	11.0	4.2	3.7
2	8.1	15.7	15.8	8.2	3.9	3.7
3	7.5	15.2	15.3	8.5	4.0	3.9
4	6.8	10.8	11.1	7.0	4.4	4.0
5	6.6	11.0	11.1	7.3	4.7	3.6
6	5.5	12.2	12.2	7.2	3.9	3.8
7	5.2	12.8	12.9	6.3	4.9	4.8
8	7.0	11.1	11.5	6.8	7.0	5.6
9	6.4	9.2	9.6	7.3	8.5	7.3
10	4.8	8.6	8.7	6.9	6.4	5.4
Average (1 standard deviation)	4.6 (1.3)	8.0 (2.4)	8.3 (2.4)	4.5 (1.3)	3.7 (1.6)	3.4 (1.2)
Greater Vancouver Region						
1	3.7	5.5	5.7	3.4	3.3	2.7
2	3.7	5.5	5.7	2.5	2.5	2.3
3	4.3	6.6	6.7	2.2	2.1	2.0
4	3.4	9.3	9.3	4.0	2.4	2.2
5	3.8	5.5	5.6	2.9	2.8	2.3
6	4.2	6.3	6.4	2.2	2.1	2.0
7	3.2	7.1	7.1	3.5	2.2	2.1
8	3.3	5.4	5.6	5.5	4.6	3.4
9	3.2	4.9	5.3	4.7	4.8	3.9
10	2.6	4.3	4.5	4.3	2.8	2.9
Average (1 standard deviation)	3.2 (0.5)	5.4 (1.4)	5.6 (1.3)	3.1 (1.1)	2.7 (1.0)	2.4 (0.6)

*Geometric mean of two horizontal components.
†Root sum of squares of two horizontal components.
‡Root sum of squares of three components.

earthquake corresponds to MMI IV–V. The basin structure model does not include soft sediments ($V_S < 625$ m/s) or surface topography, which may also amplify ground shaking. For reference, PGV at stiff soil sites in the Seattle basin region correspond to MMI IV from the M_w 6.8 Nisqually earthquake, which caused U.S. $2 billion worth of damage in Washington. The average maximum increase in peak motion due to basin structure in south Greater Vancouver is a factor of 3.1.

The proposed predictor variable for basin amplification is the depth to either a V_S of 1.0 ($Z_{1.0}$), 1.5 ($Z_{1.5}$), or 2.5 ($Z_{2.5}$) km/s, in which $Z_{1.5}$ is preferred for the LA basin (Day *et al.*, 2008). To investigate which proposed predictor variable may be applicable to the Georgia basin, the overall average basin amplification map is compared with isodepth contours of 1.0, 1.5, and 2.5 km/s sediments in the basin structure model in Figure 13. The area of highest basin amplification (3–4) is primarily associated with the lowest velocity sediments in the upper 1 km, that is, $Z_{1.0}$ at 250 m depth and $Z_{1.5}$ at 500 m depth. An appropriate measure of basin amplification for the Georgia basin appears to be $Z_{1.0}$ or $Z_{1.5}$, but not $Z_{2.5}$. Hence, ground-motion prediction equations that utilize $Z_{2.5}$ as the basin sediment-thickness correction term should not be used for sites within the Georgia basin. Comparisons with a short-period site correction term (e.g., V_{S30}) are not possible here due to the long-period nature of the modeling, that is, 250 m uniform grid and minimum V_S of 625 m/s.

Conclusions

To assess the effects of the 3D Georgia basin structure on long-period (>2 s) ground motion due to large earthquakes within 100 km of Greater Vancouver, numerical 3D FD modeling of viscoelastic wave propagation is carried out. This research provides the first detailed investigation of 3D earthquake ground motion for a sedimentary basin in Canada. Shorter period ground motions are not resolved, limited by the grid spacing and minimum V_S chosen for the 3D basin model according to a ≥5 node per minimum shear wavelength rule-of-thumb commonly used for fourth-order FD schemes. Overall the work presented here (and in Molnar *et al.*, 2014) represents an important step toward quantifying the effect of the Georgia basin on earthquake ground motion in southwest British Columbia.

Accuracy of the 3D FD simulations are evaluated here by comparing predicted and empirical waveforms of the 2001 M_w 6.8 Nisqually earthquake; the only large good-quality empirical dataset available for the Georgia basin region. General agreement in amplitude and phase of first

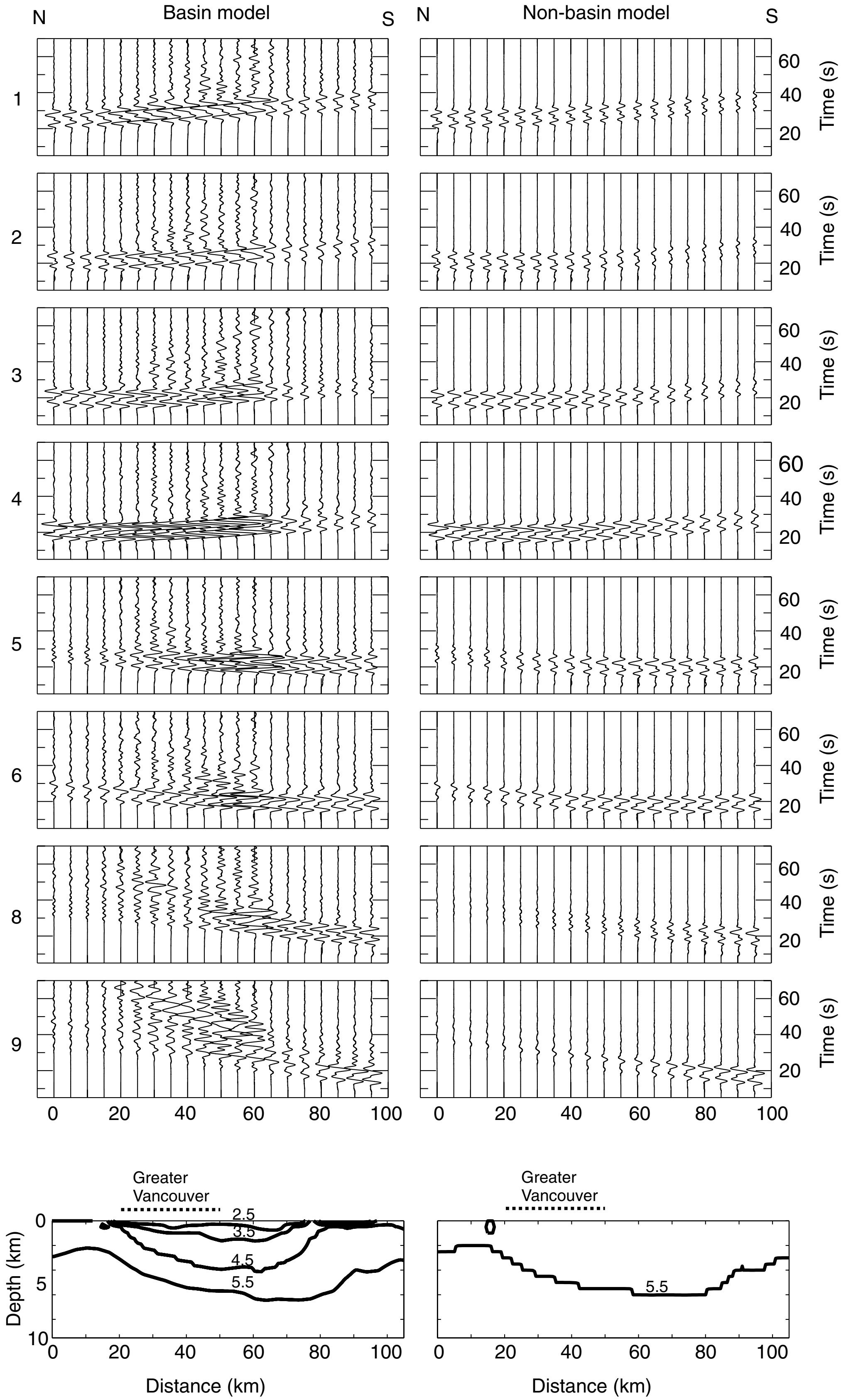

Figure 10. Synthetic basin and nonbasin east–west component waveforms for eight selected scenario earthquakes along the north–south profile shown in Figure 7. The bottom panels shows the corresponding vertical cross sections of the basin and nonbasin models (contours of V_P, km/s are labeled) to 10 km depth.

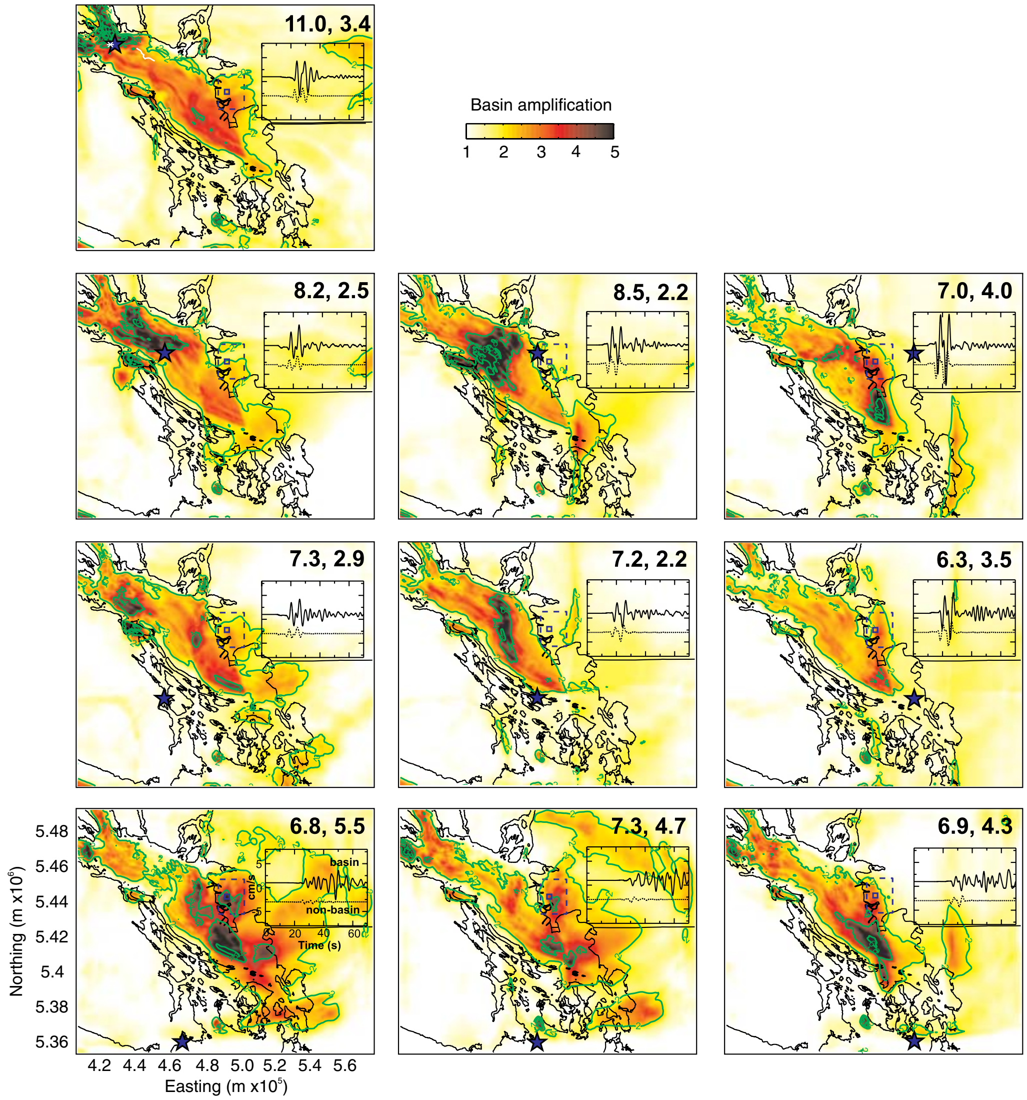

Figure 11. Maps of basin amplification for all 10 scenario earthquakes; stars show epicenter locations, and the coastline and international border are shown by black lines. Numbers in the upper right of each panel correspond to the maximum basin amplification factor within the Georgia basin (map area shown north of 5.38×10^6 m) and Greater Vancouver (dashed rectangle) regions. A synthetic east–west component waveform is shown in the upper right of each panel for the basin (upper waveform) and nonbasin (lower waveform) model simulations corresponding to a location within Greater Vancouver (small square). The color version of this figure is available only in the electronic edition.

arrival *S* waves is obtained at stations in the Seattle basin within 100 km of the source; the Nisqually earthquake source-rupture model is relatively well determined from previous 3D FD simulation studies (Pitarka *et al.*, 2004; Frankel *et al.*, 2007, 2009). In this near-source region, estimates of PGV (0.2–0.4 Hz bandwidth) are biased by a factor of 1.3 (this study) and 1.1 (Frankel *et al.*, 2009) for the same physical-structure and source-rupture models; Frankel *et al.* (2009) obtain slightly better agreement by using a nonuniform FD scheme, that is, inclusion of smaller scale structure toward surface increases the accuracy of predicted long-period ground motions. For the Georgia basin region, the bias between predicted and empirical PGV is a factor of 2.1, which is reduced to a factor of 1.6 when the base Pacific Northwest velocity model is updated here with higher-resolution shallow (<1 km) geologic and geophysical datasets. Improvement in predicted low-frequency ground motions is negligible for a variety of physically reasonable *Q* relations for the lowest velocity sediments in the basin model. Overall, general agreement of waveforms in the near-source region is achieved and provides confidence in the use of the Nisqually earthquake source model to simulate large subducting JdF plate scenario earthquakes in the Georgia basin region.

A total of 10 scenario earthquakes within the subducting JdF plate (42–55 km depth) are simulated with hypocenters in realistic locations based on known seismicity. All simulated earthquakes are characterized by the same source

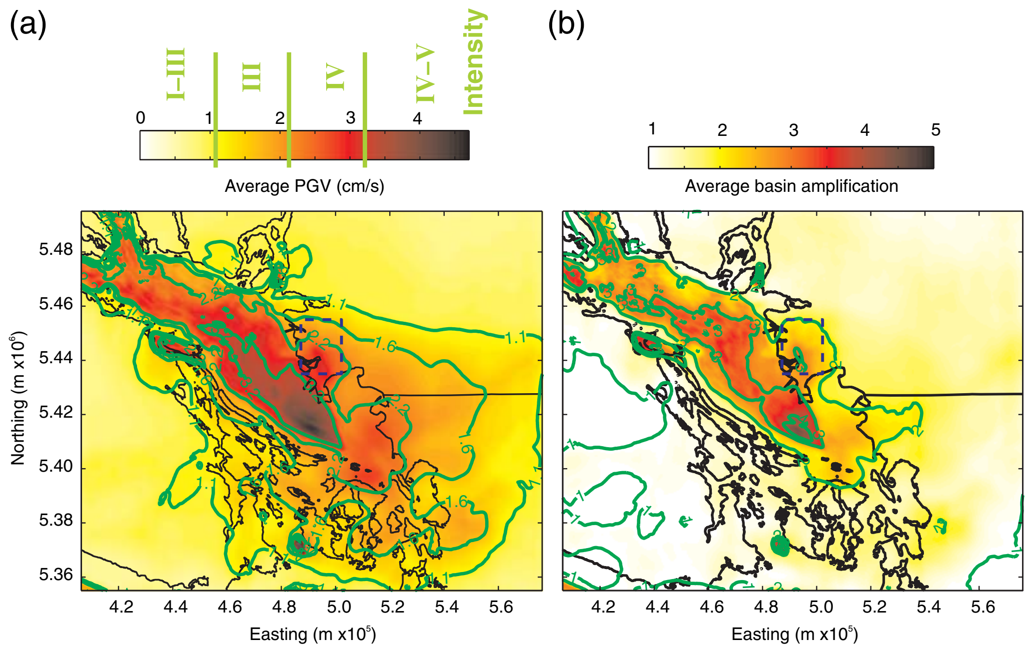

Figure 12. (a) Average PGV and (b) basin amplification for all 10 scenario earthquakes. The coastline and international border are shown by black lines. Greater Vancouver is outlined by the dashed rectangle. The color version of this figure is available only in the electronic edition.

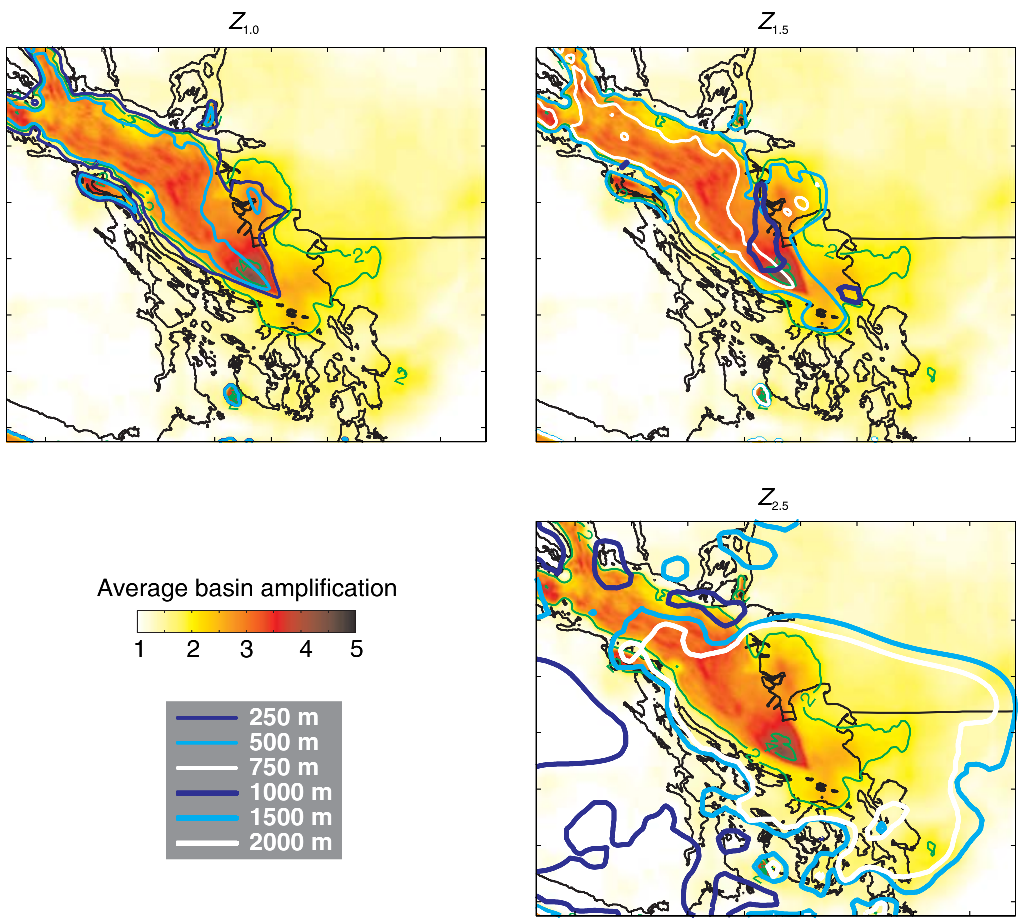

Figure 13. Average basin amplification compared to $Z_{1.0}$, $Z_{1.5}$, and $Z_{2.5}$ isodepth contours in the upper 2 km of the basin model. The coastline and international border are shown by thin black lines. The color version of this figure is available only in the electronic edition.

process of the Nisqually earthquake. Nonetheless, the FD simulations presented here provide significant insight to the expected amplification in ground shaking due to 3D basin structure. For all simulations, some general effects are observed consistently when Georgia basin sediments ($625\ \text{m/s} \le V_P < 5.5\ \text{km/s}$) are included in the 3D structure model. The symmetry of the seismic radiation pattern is distorted, and the area of higher ground motions is increased. Surface waves are generated in the southeast and northwest parts of the basin coincident with steep basin edges in the upper 1 km of the model. The average maximum peak ground motion for an M_w 6.8 JdF plate earthquake in the Georgia basin model is 4.6 cm/s (MMI V), and the average maximum basin amplification is 4.5; for the Greater Vancouver region, the average maximum PGV and basin amplification is 3.2 cm/s (MMI IV–V) and a factor of 3.1, respectively. Overall, the highest basin amplification (largest surface waves) generated across Greater Vancouver is associated with earthquakes located ≥80 km south-southwest of the city. The area of basin-amplified motion (≥2.5) is primarily associated with the lowest velocity sediments ($V_S \le 1.0\ \text{km/s}$) at 250 and 500 m depth surfaces of the model.

Limitations of this work include: (1) uncertainty in accuracy of physical-structure and source-rupture models; (2) omission of low-velocity ($V_S < 625\ \text{m/s}$) materials in the 3D structure models, such as water and up to 300 m of Holocene Fraser River delta sediments, as well as surface topography; and (3) inability to resolve frequencies > 0.5 Hz. The updated 3D physical-structure model can be further improved by: (1) incorporation of the 600 m gridded V_P model of Dash *et al.* (2007; only the 800 m surface was used here), (2) validation by comparison with future empirical earthquake recordings, and (3) increasing the maximum depth to ~80 km for simulation of JdF plate earthquakes (constrained to maximum depth of 55 km here). Conclusions are limited to the simulations conducted here and are specific to the chosen epicenter locations and earthquake rupture style. However, conclusions as to the overall most hazardous deep JdF plate scenario earthquake (within 100 km of Greater Vancouver) are relatively robust because the most likely locations and rupture style of such an event have been considered here. Overall, this study shows that the presence of 3D Georgia basin structure increases the level and duration of predicted long-period ground shaking, effects that are linked to potential earthquake damage.

Data and Resources

Subvolumes of the Pacific Northwest Community Velocity Model (v. 1.3) of Stephenson (2007) are used for the 3D modeling. Velocity data supplication provided by Jim Hunter (Natural Resources Canada [NRCAN], Ottawa), Stephen Glover (British Columbia Ministry of Energy, Mines and Petroleum Resources), David Mosher (NRCAN, Atlantic), and Ranjan Dash (Chevron). Earthquake recordings of the 2001 Nisqually earthquake used in this work were retrieved from online catalogs of the Pacific Northwest Seismic Network at ftp://ftp.geophys.washington.edu/pub/seis_net/OLYMPIA/ (last accessed November 2013) and ftp://ftpext.usgs.gov/pub/cr/co/golden/hazards/Carver/Seattle/SEAascii200001to200409/20010228185444/ (last accessed November 2013) and from the Canadian National Seismic Network at http://earthquakescanada.nrcan.gc.ca/stndon/AutoDRM/autodrm_req-eng.php (last accessed March 2009). The Anelastic Wave Propagation–Olsen Day Cui (AWP–ODC) finite-difference simulation code was used for the 3D simulations. Software used to update the 3D velocity structure model includes ArcGIS (ESRI) and ParaView (open source). Maps and time snapshots of FD simulations were generated using MATLAB (MathWorks) software; coordinates of the North American coastline were obtained at http://www.ngdc.noaa.gov/mgg/coast/ (last accessed August 2010). Waveforms filtered and plotted using Seismic Analysis Code (Incorporated Research Institutions for Seismology) software.

Acknowledgments

The authors gratefully acknowledge beneficial discussions with Garry Rogers (NRCAN, Pacific), Patrick Monahan (Penn West Exploration), Art Frankel (USGS, Washington), and Arben Pitarka (URS, California). Thank you to Robert Kung (NRCAN, Pacific) for GIS support and to the Minerva computer support staff at the University of Victoria. We gratefully acknowledge reviews by Allison Bent (NRCAN, Ottawa) and three anonymous reviewers. Funding provided by National Sciences and Engineering Research Council (NSERC) of Canada, University of Victoria, and Natural Resources Canada. This is ESS contribution 20110281.

References

Aagaard, B. T., T. M. Brocher, D. Dolenc, D. Dreger, R. W. Graves, S. Harmsen, S. Hartzell, S. Larsen, and M. L. Zoback (2008a). Ground-motion modeling of the 1906 San Francisco earthquake, Part I: Validation using the 1989 Loma Prieta earthquake, *Bull. Seismol. Soc. Am.* **98,** 989–1011.

Aagaard, B. T., T. M. Brocher, D. Dolenc, D. Dreger, R. W. Graves, S. Harmsen, S. Hartzell, S. Larsen, K. McCandless, S. Nilsson, N. A. Petersson, A. Rodgers, B. Sjögreen, and M. L. Zoback (2008b). Ground-motion modeling of the 1906 San Francisco earthquake, Part II: Ground-motion estimates for the 1906 earthquake and scenario events, *Bull. Seismol. Soc. Am.* **98,** 1012–1046.

Aagaard, B. T., R. W. Graves, A. Rodgers, T. M. Brocher, R. W. Simpson, D. Dreger, N. A. Petersson, S. C. Larsen, S. Ma, and R. C. Jachens (2010). Ground-motion modeling of the Hayward fault scenario earthquakes, Part II: Simulation of long-period and broadband ground motions, *Bull. Seismol. Soc. Am.* **100,** 2945–2977.

Aagaard, B. T., R. W. Graves, D. P. Schwartz, D. A. Ponce, and R. W. Graymer (2010). Ground-motion modeling of Hayward fault scenario earthquakes, Part I: Construction of the suite of scenarios, *Bull. Seismol. Soc. Am.* **100,** 2927–2944.

Adams, J. A., and S. Halchuk (2003). Fourth generation seismic hazard maps of Canada: Values for over 650 Canadian localities intended for the 2005 National Building Code of Canada, *Geol. Surv. Canada Open-File Rept. 4459*, 155 pp.

American Society of Civil Engineers (ASCE) (2006). *Minimum Design Loads for Buildings and Other Structures, Standards ASCE/SEI 7-05*, ISBN: 9780784408094, 420 pp.

American Society of Civil Engineers (ASCE) (2010). *Minimum Design Loads for Buildings and Other Structures, Standards ASCE/SEI 7-10*, ISBN: 9780784410851, 650 pp.

Aoi, S., R. Honda, N. Morikawa, H. Sekiguchi, H. Suzuki, Y. Hayakawa, T. Kunugi, and H. Fujiwara (2008). Three-dimensional finite difference simulation of long-period ground motions for the 2003 Tokachi-oki, Japan, earthquake, *J. Geophys. Res.* **113,** doi: 10.1029/2007JB005452.

Bard, P.-Y., and M. Bouchon (1980). The two-dimensional resonance of sediment-filled valleys, *Bull. Seismol. Soc. Am.* **75,** 519–541.

Bielak, J., R. W. Graves, K. B. Olsen, R. Taborda, L. Ramírez-Guzmán, S. M. Day, G. P. Ely, D. Roten, T. H. Jordan, P. J. Maechling, J. Urbanic, Y. Cui, and G. Juve (2010). The ShakeOut earthquake scenario: Verification of three simulation sets, *Geophys. J. Int.* **180,** 375–404.

Bolton, M. K. (2003). Juan de Fuca plate seismicity at the northern end of the Cascadia subduction zone, *M. Sc. Thesis*, University of Victoria, Victoria, British Columbia.

Brocher, T. M. (2007). Key elements of regional seismic velocity models for long period ground motion simulations, *J. Seismol.*, doi: 10.1007/s10950-007-9061-3.

Brocher, T. M. (2008). Compressional and shear-wave velocity versus depth relations for common rock types in northern California, *Bull. Seismol. Soc. Am.* **98,** 950–968.

Bustin, A., R. D. Hyndman, A. Lambert, J. Ristau, J. He, H. Dragert, and M. Van der Kooij (2004). Fault parameters of the Nisqually earthquake determined from moment tensor solutions and the surface deformation from GPS and InSAR, *Bull. Seismol. Soc. Am.* **94,** 363–376.

Cassidy, J. F., and G. C. Rogers (1999). Seismic site response in the greater Vancouver, British Columbia, area: spectral ratios from moderate earthquakes, *Can. Geotech. J.* **36,** 195–209.

Cassidy, J. F., and G. C. Rogers (2004). Variation in ground shaking on the Fraser River delta (Greater Vancouver, Canada) from analysis of moderate earthquakes, in *Proc. 14th World Conference on Earthquake Engineering*, Vancouver, British Columbia, 1–6 August 2004, Paper 1010.

Cassidy, J. F., A. Rosenberger, and G. C. Rogers (2008). Strong motion seismograph networks, data, and research in Canada, in *Proc. of the 14th World Conference on Earthquake Engineering*, Beijing, China, 12–17 July 2008.

Cerjan, C., D. Kosloff, R. Kosloff, and M. Reshef (1985). Absorbing boundary conditions for acoustic and elastic wave equations, *Bull. Seismol. Soc. Am.* **67,** 1529–1540.

Clayton, R., and B. Engquist (1977). Absorbing boundary conditions for acoustic and elastic wave equations, *Bull. Seismol. Soc. Am.* **67,** 1529–1540.

Collino, F., and C. Tsogka (2001). Application of the PML absorbing layer model to the linear elastodynamic problem in anisotropic heterogeneous media, *Geophysics* **66,** 294–307.

Dash, R. K., G. D. Spence, M. Riedel, R. D. Hyndman, and T. M. Brocher (2007). Upper-crustal structure beneath the Strait of Georgia, Southwest British Columbia, *Geophys. J. Int.* **170**, 800–802, doi: 10.1111/j.1365-246X.2007.03455.x.

Day, S. M. (1998). Efficient simulation of constant Q using coarse-grained memory variables, *Bull. Seismol. Soc. Am.* **88,** 1051–1062.

Day, S. M., and C. R. Bradley (2001). Memory-efficient simulation of anelastic wave propagation, *Bull. Seismol. Soc. Am.* **91,** 520–531.

Day, S. M., R. Graves, J. Bielak, D. Dreger, S. Larsen, K. B. Olsen, A. Pitarka, and L. Ramirez-Guzman (2008). Model for basin effects on long-period response spectra in southern California, *Earthq. Spectra* **24,** 257–277.

England, T. D. J., and R. M. Bustin (1998). Architecture of the Georgia basin, southwestern British Columbia, *Bull. Can. Petrol Geol.* **46,** 288–320.

Finn, W. D. L., E. Zhai, T. Thavaraj, X.-S. Hao, and C. E. Ventura (2003). 1-D and 2-D analyses of weak motion data in Fraser Delta from 1996 Duvall earthquake, *Soil Dynam Earthq. Eng.* **23,** 323–329.

Frankel, A. (1993). Three-dimensional simulations of ground motions in the San Bernardino valley, California, for hypothetical earthquakes on the San Andreas fault, *Bull. Seismol. Soc. Am.* **83,** 1020–1041.

Frankel, A., and W. Stephenson (2000). Three-dimensional simulations of ground motions in the Seattle region for earthquakes in the Seattle fault zone, *Bull. Seismol. Soc. Am.* **90,** 1251–1267.

Frankel, A., and J. Vidale (1992). A three-dimensional simulation of seismic waves in the Santa Clara valley, California, from a Loma Prieta aftershock, *Bull. Seismol. Soc. Am.* **82,** 2045–2074.

Frankel, A. D., W. Stephenson, and D. Carver (2009). Sedimentary basin effects in Seattle, Washington: Ground-motion observations and 3D simulations, *Bull. Seismol. Soc. Am.* **99,** 1579–1611.

Frankel, A. D., W. J. Stephenson, D. L. Carver, R. A. Williams, J. K. Odom, and S. Rhea (2007). Seismic hazard maps for Seattle incorporating 3D sedimentary basin effects, nonlinear site response, and rupture directivity, *U.S. Geol. Surv. Open-File Rept. 2007-1175*, 77 pp.

Furumura, T., and S. K. Singh (2002). Regional wave propagation from Mexican subduction zone earthquakes: The attenuation functions for interplate and inslab events, *Bull. Seismol. Soc. Am.* **92,** 2110–2125.

Furumura, T., K. Koketsu, and K. L. Wen (2002). Parallel PSM/FDM hybrid simulation of ground motions from the 1999 Chi-Chi, Taiwan, earthquake, *Pure Appl. Geophys.* **159,** 2133–2146.

Graves, R. W., and B. T. Aagaard (2011). Testing long-period ground-motion simulations of scenario earthquakes using the M_w 7.2 El Mayor-Cucapah mainshock: Evaluation of finite-fault rupture characterization and 3D seismic velocity models, *Bull. Seismol. Soc. Am.* **101,** 895–907.

Graves, R. W., and A. Pitarka (2004). Broadband time history simulation using a hybrid approach, in *Proc. 13th World Conference on Earthquake Engineering*, Vancouver, British Columbia, 1–6 August 2004, Paper 1098.

Graves, R. W., A. Pitarka, and P. Sommerville (1998). Ground-motion amplification in the Santa Monica area: Effects of shallow basin-edge structure, *Bull. Seismol. Soc. Am.* **88,** 1224–1242.

Halchuk, S., and J. A. Adams (2004). Deaggregation of seismic hazard for selected Canadian cities, in *Proc. 13th World Conference on Earthquake Engineering*, Vancouver, British Columbia, 1–6 August 2004, Paper 2470.

Hamilton, T. S. (1991). Seismic stratigraphy of unconsolidated sediments in the central Strait of Georgia: Hornby Island to Roberts Bank, *Geol. Surv. Canada Open-File Rept. 2530* (9 sheets).

Hannigan, P. K., J. R. Dietrich, P. J. Lee, and K. G. Osadetz (2001). Petroleum resource potential of sedimentary basins on the Pacific margin of Canada, *Geol. Surv. Canada Bull.* **564,** 72 pp.

Harris, J. B., J. A. Hunter, J. L. Luternauer, and W. D. L. Finn (1998). Site amplification modelling of the Fraser Delta, British Columbia, in *Geology and Natural Hazards of the Fraser River Delta, British Columbia*, J. J. Clague, J. L Luternauer, and D. C Mosher (Editors), Geol. Surv. Canada Bull., Vol. 525, 211–216.

Hartzell, S., A. Frankel, P. Liu, Y. Zeng, and S. Rahman (2011). Model and parametric uncertainty in source-based kinematic models of earthquake ground motion, *Bull. Seismol. Soc. Am.* **101,** 2431–2452.

Hartzell, S., S. Harmsen, and A. Frankel (2010). Effects of random correlated velocity perturbations on predicted ground motions, *Bull. Seismol. Soc. Am.* **100,** 1415–1426.

Hartzell, S., A. Leeds, A. Frankel, R. Williams, J. Odum, W. Stephenson, and W. Silva (2002). Simulations of broadband ground motions including nonlinear soil effects for a magnitude 6.5 earthquake on the Seattle fault, Seattle, Washington, *Bull. Seismol. Soc. Am.* **92,** 831–853.

Hyndman, R. D., G. C. Rogers, H. Dragert, K. Wang, J. J. Clague, J. Adams, and P. T. Bobrowsky (1996). Giant earthquakes beneath Canada's west coast, *Geosci. Can.* **23,** 63–72.

Ichinose, G. A., H. K. Thio, and P. G. Somerville (2004). Rupture process and near-source shaking of the 1965 Seattle-Tacoma and 2001 Nisqually, intraslab earthquakes, *Geophys. Res. Lett.* **31,** doi: 10.1029/2004GL019668.

Ichinose, G. A., H. K. Thio, and P. G. Somerville (2006). Moment tensor and rupture model for the 1949 Olympia, Washington, earthquake and scaling relations for Cascadia and global intraslab earthquakes, *Bull. Seismol. Soc. Am.* **96,** 1029–1037.

Iwaki, A., and T. Iwata (2010). Simulation of long-period ground motion in the Osaka sedimentary basin: performance estimation and the basin structure effects, *Geophys. J. Int.* **181,** 1062–1076.

Kao, H., K. Wang, R.-Y. Chen, I. Wada, J. He, and S. D. Malone (2008). Identifying the rupture place of the 2001 Nisqually, Washington, earthquake, *Bull. Seismol. Soc. Am.* **98,** 1546–1558.

Kawase, H. (1996). The cause of the damage belt in Kobe: 'The basin-edge effect', constructive interference of the direct *S* wave with the basin-induced diffracted/Rayleigh waves, *Seismol. Res. Lett.* **67,** 25–35.

Lee, S.-J., H.-W. Chen, and B.-S. Huang (2008). Simulations of strong ground motion and 3D amplification effect in the Taipei basin by using a composite grid finite-difference method, *Bull. Seismol. Soc. Am.* **98,** 1229–1242.

Lee, S.-J., D. Komatitsch, B.-S. Huang, and J. Tromp (2009). Effects of topography on seismic-wave propagation: An example from northern Taiwan, *Bull. Seismol. Soc. Am.* **99,** 314–325.

Levander, A. R. (1988). Fourth-order finite-difference P-SV seismograms, *Geophysics* **53,** 1425–1436.

Liu, P.-C., and R. J. Archuleta (2002). The effect of a low-velocity surface layer on simulated ground motion, *Seismol. Res. Lett.* **73,** 267.

Lowe, C., S. A. Dehler, and B. C. Zelt (2003). Basin architecture and density structure beneath the Strait of Georgia, British Columbia, *Can. J. Earth Sci.* **40,** 965–981.

Ludwig, W. J., J. E. Nafe, and C. L. Drake (1970). Seismic refraction, in *The Sea*, A. E. Maxwell (Editor), Wiley-Interscience, New York, 53–84.

Magistrale, H., K. McLaughlin, and S. Day (1996). A geology based 3-D velocity model of the Los Angeles basin sediments, *Bull. Seismol. Soc. Am.* **86**, 1161–1166.

Marcinkovich, C., and K. Olsen (2003). On the implementation of perfectly matched layers in a three-dimensional fourth-order velocity-stress finite difference scheme, *J. Geophys. Res.* **108**, no. B5, doi: 10.1029/2002JB002235.

Miksat, J.,, K.-L. Wen, F. Wenzel, V. Sokolov, and C.-T. Chen (2010). Numerical modelling of ground motion in the Taipei basin: basin and source effects, *Geophys. J. Int.* **183,** 1633–1647.

Moczo, P., J. Kristek, and L. Halada (2000). 3D fourth-order staggered-grid finite-difference schemes: Stability and grid dispersion, *Bull. Seismol. Soc. Am.* **90,** 587–603.

Molnar, S. (2011). Predicting earthquake ground shaking due to 1D soil layering and 3D basin structure in SW British Columbia, Canada, *Ph.D. Thesis*, University of Victoria, Victoria, British Columbia, 150 pp.

Molnar, S., J. F. Cassidy, S. E. Dosso, and K. B. Olsen (2008). Seismic hazard investigations of southwestern British Columbia, Canada, in *14th World Conference on Earthquake Engineering*, Beijing, China, 12–17 October 2008, Poster 214.

Molnar, S., J. F. Cassidy, S. E. Dosso, and K. B. Olsen (2010). 3D Ground motion in the Georgia basin region of SW British Columbia for Pacific Northwest scenario earthquakes, in *Proc. 9th U.S. National and 10th Canadian Conference on Earthquake Engineering*, Toronto, Ontario, Paper 754.

Molnar, S., J. F. Cassidy, K. B. Olsen, S. E. Dosso, and J. He (2014). Earthquake ground motion and 3D Georgia basin amplification in Southwest British Columbia: Shallow blind-thrust scenario earthquakes *Bull. Seismol. Soc. Am.* **104,** no. 1, doi: 10.1785/0120130116.

Mosher, D. C., and T. S. Hamilton (1998). Morphology, structure and stratigraphy of the offshore Fraser Delta and adjacent Strait of Georgia, in *Geology and Natural Hazards of the Fraser River Delta, British Columbia*, J. J. Clague, J. L. Lautenauer, and D. C. Mosher (Editors), Geological Survey of Canada, Bulletin, Vol. 525, 147–160.

Mustard, P. S. (1994). The Upper Cretaceous Nanaimo Group, Georgia basin, in *Geology and Geological Hazards of the Vancouver Region, Southwestern British Columbia*, J. W. H. Monger (Editor), Geological Survey of Canada, Bulletin 481, 27–95.

NEHRP Consultants Joint Venture (2011). NEHRP Consultants Joint Venture Report: Selecting and scaling earthquake ground motions for performing response-history analyses, Report Number NIST GCR 11-917-75, U.S. Department of Commerce, National Institute of Standards and Technology, November 2011, 256 pp.

Olsen, K. B. (1994) Simulation of three-dimensional wave propagation in the Salt Lake Basin, *Ph.D. Thesis*, University of Utah, Salt Lake City, Utah, 157 pp.

Olsen, K. B. (2000a). 3D Viscoelastic wave propagation in the Upper Borrego valley, California, constrained by borehole and surface data, *Bull. Seismol. Soc. Am.* **90,** 134–150.

Olsen, K. B. (2000b). Site amplification in the Los Angeles basin from three dimensional modeling of ground motion, *Bull. Seismol. Soc. Am.* **90,** S77–S94.

Olsen, K. B. (2003). Estimation of Q for long-period (>2 sec) waves in the Los Angeles basin, *Bull. Seismol. Soc. Am.* **93,** 627–638.

Olsen, K. B., and R. J. Archuleta (1996). Three-dimensional simulation of earthquakes on the Los Angeles fault system, *Bull. Seismol. Soc. Am.* **86,** 575–596.

Olsen, K. B., and G. T. Schuster (1994). Three-dimensional modeling of site amplification in East Great Salt Lake Basin, *U.S. Geol. Surv. Tech. Rept. 1434-93-G-2345*, 102 pp.

Olsen, K. B., J. C. Pechmann, and G. T. Schuster (1995). Simulation of 3D elastic wave propagation in the Salt Lake basin, *Bull. Seismol. Soc. Am.* **85,** 1688–1710.

Olsen, K. B., W. J. Stephenson, and A. Geisselmeyer (2008). 3D Crustal structure and long-period ground motions from a M9.0 megathrust earthquake in the Pacific Northwest region, *J. Seismol.* **12,** 145–159.

Onur, T., S. Molnar, J. Cassidy, C. E. Ventura, and K. X.-S. Hao (2004). Estimating site periods in Vancouver and Victoria, British Columbia using microtremor measurements and SHAKE analyses, in *Canadian Geotechnical Conference*, Quebec City, Quebec, 24–27 October 2004, 8 pp.

Onur, T., C. E. Ventura, and W. D. L. Finn (2005). Regional seismic risk in British Columbia—Damage and loss distribution in Victoria and Vancouver, *Can. J. Civ. Eng.* **32,** 361–371.

Pitarka, A. (1999). 3D elastic finite-difference modelling of seismic motion using staggered grids with non-uniform spacing, *Bull. Seismol. Soc. Am.* **89,** 54–68.

Pitarka, A., R. Graves, and P. Somerville (2004). Validation of a 3D velocity model of the Puget Sound region based on modeling ground motion from the 28 February 2001 Nisqually earthquake, *Bull. Seismol. Soc. Am.* **94,** 1670–1689.

Pitarka, A., K. Irikura, and T. Iwata (1997). Modeling of ground motion in the Higashinada (Kobe) area for an aftershock of the 1995 January 17 Hyogo-ken Nanbu, Japan, earthquake, *Geophys. J. Int.* **131,** 2, 231–239.

Ramachandran, K., S. E. Dosso, C. A. Zelt, G. D. Spence, R. D. Hyndman, and T. M. Brocher (2004). Upper crustal structure of southwestern British Columbia from the 1998 Seismic Hazards Investigation in Puget Sound, *J. Geophys. Res.* **109,** doi: 10.1029/2003JB002826.

Ramachandran, K., R. D. Hyndman, and T. M. Brocher (2006). Regional P wave velocity structure of the northern Cascadia subduction zone, *J. Geophys. Res.* **111,** doi: 10.1029/2005JB004108.

Ristau, J., G. C. Rogers, and J. F. Cassidy (2007). Stress in western Canada from regional moment tensor analysis, *Can. J. Earth Sci.* **44,** 127–148.

Rogers, G. C. (1998). Earthquakes and earthquake hazard in the Vancouver area, in *Geology and Natural Hazards of the Fraser River Delta, British Columbia*, J. J. Clague, J. L. Luternauer, and D. C. Mosher (Editors), Geological Survey of Canada, Bulletin, Vol. 525, 17–25.

Roullé, A., and F. J. Chávez-García (2006). The strong ground motion in Mexico City: Analysis of data recorded by a 3D array, *Soil. Dynam. Earthq. Eng.* **26,** 71–89.

Singh, S. K., E. Mena, and R. Castro (1988). Some aspects of the source characteristics and ground motion amplifications in and near Mexico city from acceleration data of the September 1985, Michoacan, Mexico earthquakes, *Bull. Seismol. Soc. Am.* **78,** 451–477.

Stephenson, W. J. (2007). Velocity and density models incorporating the Cascadia subduction zone for 3D earthquake ground motion simulations, version 1.3, *U.S. Geol. Surv. Open-File Rept. 2007-1348*, 24 pp.

Stephenson, W. J., A. D. Frankel, J. K. Odum, R. A. Williams, and T. L. Pratt (2006). Towards resolving an earthquake ground motion mystery in west Seattle, Washington state: Shallow seismic focusing may cause anomalous chimney damage, *Geophys. Res. Lett.* doi: 10.1029/2005GL025037.

White, D. J., and R. M. Clowes (1984). Seismic investigation of the Coast plutonic complex—Insular belt boundary beneath the Strait of Georgia, *Can. J. Earth Sci.* **21,** 1033–1049.

Wiest, K. R., D. I. Doser, A. A. Velasco, and J. Zollweg (2007). Source inversion and comparison of the 1939, 1946, 1949 and 1965 earthquakes, Cascadia subduction zone, western Washington, *Pure Appl. Geophys.* **164,** 1905–1919.

Worden, C. B., M. C. Gerstenberger, D. A. Rhoades, and D. J. Wald, (2012). Probabilistic relationships between ground-motion parameters and modified Mercalli intensity in California, *Bull. Seismol. Soc. Am.* **102,** 204–221.

Zelt, B. C., R. M. Ellis, C. A. Zelt, R. D. Hyndman, C. Lowe, G. D. Spence, and M. A. Fisher (2001). Three-dimensional crustal velocity structure beneath the Strait of Georgia, British Columbia, *Geophys. J. Int.* **144,** 695–712.

University of Victoria
School of Earth and Ocean Sciences
3800 Finnerty Road
Victoria, British Columbia V8P 5C2
smolnar@uvic.ca
sdosso@uvic.ca
(S.M., S.E.D.)

Natural Resources Canada
P.O. Box 6000
Sidney, British Columbia V8L 4B2
jcassidy@nrcan.gc.ca
jhe@nrcan.gc.ca
(J.F.C., J.H.)

San Diego State University
Department of Geological Sciences
GMCS 231A
5500 Campanile Dr
San Diego, California 92182-1020
kbolsen@mail.sdsu.edu
(K.B.O.)

Manuscript received 30 September 2011;
Published Online 21 January 2014